Using fractals to describe ecologically-relevant patterns in distributions of large rocks in streams

Authors: G. K. Dwyer[1], C. R. Cummings[1], S. P. Rice[2], Jill Lancaster[3], Barbara J. Downes[3], L. Slater[4], and Rebecca E. Lester[1]

[1]Centre for Regional and Rural Futures, Deakin University, Locked Bag 20000, Geelong, Vic. 3220, Australia.

[2] Department of Geography and Environment, Loughborough University, Loughborough, LE11 3TU, U.K.

[3] School of Geography, The University of Melbourne, Victoria, Australia

[4]School of Geography and the Environment, University of Oxford, South Parks Road, Oxford OX1 3QY, UK

Corresponding author: Rebecca Lester (Rebecca.Lester@deakin.edu.au)

Key Points:

- Longitudinal patterns of emergent fluvial rocks in six streams in Scotland and Australia exhibited fractal behaviour (self-similarity).
- Fractal dimensions were related to development of bedform topography and the density and size of available bed materials in the streams.
- Fractal dimensions are a promising measure of physical complexity that enable comparisons across ecosystems, scales and linked disciplines like ecology and geomorphology.

Supplementary material references: [*Basharin*, 1959; *Miller*, 1955; *Seuront*, 2009; *Seuront and Lagadeuc*, 1997; *Strobl*, 2005]

Abstract:

Measuring the physical complexity of habitats or ecological resources is often achieved using system-specific methods that make comparisons across ecosystems difficult. One measure that is applicable across multiple ecosystems and scales is the fractal dimension, which has the benefit of generality as well as potential scale independence. This study evaluated the use of box-counting and entropy fractal dimensions for characterising the complexity of emergent rock distributions in six streams across Scotland and Australia. Emergent rocks (ER) are important hydraulic features and ecological resources, including as oviposition sites for aquatic insects and cover for fish. We complete fractal analysis on counts of ER in 5-m segments along longitudinal stretches of the six streams. All six streams exhibited fractal behaviour (self-similarity), suggesting that fractals can be used to measure the complexity of longitudinal ER distributions in a way that is scale independent. Entropy was a superior measure due to its ability to differentiate among the six streams whereas box-counting could not. Together, field results and numerical simulations showed that fractal dimensions of emergent rock distributions were related to stream geomorphology. Well-developed bedforms, like alternating pools and riffles had better organised emergent rocks because large bed materials were more likely to be emergent in topographic highs. Streams with coarser bed materials had more chaotic arrangements of emergent rocks because this increased the general abundance of emergent rocks, making differentiation between topographic highs and lows less distinctive. Fractal dimensions, therefore, can measure the complexity of river systems in a way that is relevant to geomorphological and ecological processes.

Plain language summary:

Fractal dimensions are used to characterise the complexity of a wide range of patterns in nature, from single objects (e.g. branched twigs) to whole environments (rainforests), and learn where consistent patterns may occur. We measured the complexity of rock patterns (specifically rocks that emerge above the water’s surface) in six rivers from Scotland and Australia using fractal dimensions. These rocks provide important habitat for plants, insects, and fish in rivers, and so are important to overall stream condition and functioning. Less complex, more highly structured rock patterns (lower fractal dimensions) occurred in streams with smaller rocks, which had areas where emergent rocks were concentrated (riffles) and many long pools without emergent rocks. These results suggest that fractal dimensions may be a promising measure of complexity that can help us understand relationships between

physical characteristics of streams and their ecology. Fractal dimensions also allow comparison of rock patterns in rivers with other habitats, such as shrubs in grasslands for example. This may allow future research to explain patterns that are consistent across these different ecosystems and so advance general ecological theory.

Index terms:

1. 1825 Geomorphology: fluvial (1625)
2. 0458 Limnology (1845, 4239, 4942)
3. 1856 River channels (0483, 0744)
4. 0439 Ecosystems, structure and dynamics (4815)
5. 0430 Computational methods and data processing

Keywords:

1. Ecological resources
2. Fluvial geomorphology
3. Large roughness elements
4. Habitat complexity
5. Spatial heterogeneity
6. Information dimension

Abbreviations:

ER - Emergent rocks
D_X - Fractal dimension, unspecified method
D_B - Box-counting fractal dimension
D_E - Entropy fractal dimension
δ - Box size
LZS - synthetic low-zero streams
HZS - synthetic high-zero streams

1. Introduction

The physical structure of environments affects every aspect of ecosystem structure and function [e.g. *Cuthbert et al.*, 2019; *Ossola et al.*, 2016]. Physical structure here refers to the three-dimensional configuration of living space: rocky coasts are more physically complex than sandy beaches, forests are more physically complex than grassy plains, and so forth [*Bell et al.*, 2012]. Increasing physical complexity creates a greater diversity of resources (e.g. living spaces and food) and results in higher species diversity; this association holds true in every ecosystem that has been tested [*Barnes et al.*, 2013] and requires an explanation, but quantifying physical complexity is difficult. Most researchers address this difficulty by developing measures that are intrinsic to particular ecosystems, such as counts of cracks and crevices in rocks [*Downes et al.*, 1998], wood loading in streams [*Lester et al.*, 2007], or tributaries across networks [*Rice*, 2017]. Such eclectic measures, while useful within a system, cannot be applied across multiple ecosystems at different scales, thereby precluding general tests of hypotheses and meta-analyses.

General methods for capturing physical complexity exist and one such measure, the fractal dimension [*Mandelbrot*, 1967], is applicable across multiple ecosystems and scales. Fractal dimensions lie between the well-understood dimensions of 1, 2 and 3 for a line, surface and volume, respectively, and express the extent to which the space is filled. For example, a complex, wiggly line on a 2-dimensional plane (fractal dimension close to 2) would have a larger fractal dimension than a straight line (fractal dimension would be 1 for a perfectly straight line). While natural systems commonly require more than a single exponent to describe their dynamics (multiple scaling; multifractal), one compelling aspect of fractal dimensions is that many environments have the same fractal dimension over a range of spatial scales, in which case they are termed self-similar over those scales [*Mandelbrot*, 1967]. Coastlines [*Mandelbrot*, 1967] and river networks [*Mantilla et al.*, 2010] are two well-known examples, i.e. their maps look the same regardless of the scale at which they are mapped (self-similarity). Where environments are self-similar (fractal-like), fractal dimensions can be used to measure complexity in a way that is scale independent and transferable across ecosystem types.

Fractal dimensions and related functions have proven useful for describing characteristics of river systems, from channel networks [*Rinaldo et al.*, 1992; *Rodríguez-Iturbe and Rinaldo,* 2001; *Tarboton*, 1989; *Yang and Shi*, 2017], through riverbed topography [*Sapozhnikov and*

Foufoula-Georgiou, 1996; *Zhong et al.*, 2012] and planform sinuosity [e.g. *Nikora*, 1991] to grain-scale topography [e.g. *Butler et al.*, 2001] in one, two and three dimensions. Fractal descriptions have, in turn, offered new insights into fluvial processes, including the generation of bed material fabrics and bedforms, sediment transport, hydraulic resistance and hyporheic exchange [*Aubeneau et al.*, 2015; *Lee et al.*, 2020; *Singh et al.*, 2011; *Singh et al.*, 2009; *Stewart et al.*, 2019]. Work using fractals to describe fluvial processes has extended into descriptions of the areal arrangement of large clasts as pebble clusters [*Wu et al.*, 2018], but has not been applied to regional (comparisons among streams) or local (comparisons among habitat types within a stream) scales at which most theoretical ecological models apply [*Wiens*, 1989]. Most applications of fractals by ecologists have been over small spatial scales [e.g. *Jeffries*, 1993; *Warfe et al.*, 2008], which are less suited to understanding populations.

An outstanding question is whether physical resources for insect populations, namely rocks that protrude above the surface of the water (emergent rocks, ER) exhibit fractal arrangements. Emergent rocks are an important resource for many ovipositing insects, which rely on them for successful recruitment [*Lancaster et al.*, 2010]. They also serve as sites for insect emergence [*Petersen and Hildrew*, 2003] and as substrates for bryophytes [*Downes et al.*, 2003]. They create flow structures that provide resting, cover and feeding opportunities for fish [*Hayes and Jowett*, 1994], trap drifting organic foodstuffs [*Hoover et al.*, 2006], and create microscale habitat heterogeneity that affects the distribution of macroinvertebrates [*Bouckaert and Davis*, 1998]. The spatial arrangement of ER has ecological implications. For example, some caddisflies (*Ulmerochorema* spp.) lay eggs on ER surrounded by fast flow; such ER are typically clumped in areas of high velocity (e.g. riffles) and this can lead to very high local densities of caddisfly eggs and potentially of newly hatched larvae [*Lancaster et al.*, 2003; *Lancaster et al.*, 2020].

ER also have important roles in stream geomorphology and hydraulics, including affecting drag and shear stress [e.g. *Cooper et al.*, 2013], generating turbulent structures [e.g. *Lacey and Roy*, 2008], and influencing sediment entrainment, deposition and transport processes [e.g. *Monsalve et al.*, 2017; *Papanicolaou et al.*, 2018]. The spatial distribution of ER reflects patterns of sediment supply, dispersal, and sorting across multiple scales. The location of sediment supply points, the volume and size of sediments delivered to the channel, and subsequent sorting by particle size and shape are affected by factors including geology, geomorphological history and hydrometeorology. At local scales, large rocks are arranged into structures via process-form feedbacks with the flow. The resulting bedforms are key components in the definition of channel morphology, e.g., cascades, step-pools, plane beds and pool-riffle sequences [*Montgomery and Buffington*, 1997]. It is reasonable to expect ER to be more prevalent in riffles and similar bedforms (steps, cascades) that preferentially store coarse sediments, and where the bed surface is elevated closer to the water surface, making emergence more likely. Particle characteristics may also affect the likelihood of emergence; larger rocks should have a greater propensity to emerge, and rock shape (platy versus equant) may influence emergence and sorting processes. At larger spatial scales, ER may be more likely in zones of coarse sediment aggradation, for example at the upstream end of sedimentary links, downstream of significant tributaries [*Rice and Church*, 1998].

Beyond such simple expectations, there is limited understanding of how numbers of ER vary in space or what controls their spatial arrangement. An ability to better describe and explain the spatial organisation of ER is therefore key to improve our understanding of geomorphological and ecological processes, such as flow resistance and species diversity. In this work, we investigated the controls driving differences in fractal dimensions of ER using numerical simulations of synthetic streams designed to manipulate key characteristics independently. Specifically, we addressed three research questions:

- *(Q1) Are longitudinal ER distributions, at scales of up to a kilometre, self-similar (fractal)?*
- *(Q2) Do fractal dimensions capture differences in ER distributions between rivers associated with differences in channel morphology and sediment characteristics?*
- *(Q3) Using synthetic streams, which aspects of stream morphology are responsible for driving differences in fractal properties?*

As fractal dimensions are influenced by the density of points (here ER) and their arrangement, see Figure 1, we hypothesised that channel morphology and sediment characteristics that increase the propensity for rocks to emerge (and hence increase the number of ER) or which describe the organisation of large rocks (into pool-riffle structure for example) would be related to fractal dimension. Larger rocks, particularly in steep, shallow streams, should be more likely to be emergent. In contrast, characteristics associated with bedform development, and hence the spatial organisation of ER, are hypothesised to be negatively correlated with fractal dimension. Bedform development should be associated with pool-riffle structure, long pools without ER or with low ER densities, riffles with high ER densities, and lower stream slopes (see Supporting Information Table S1 for detailed rationale of hypotheses).

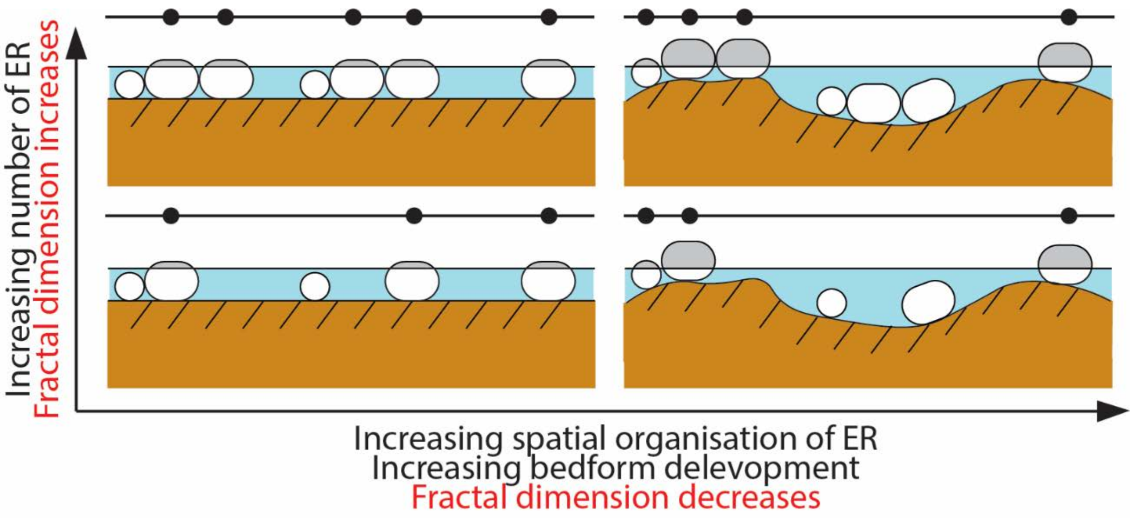

Figure 1. How channel morphology and bed sediment characteristics are expected to influence fractal dimensions. Fractal dimension is affected by the number of points and the arrangement of those points in space. The fractal dimension of a single point is 0 and a line has the well-understood dimension of 1. ER in streams are analogous to points arranged along a line. Continuing to increase the number of points or ER along the line will fill in the space until the points resemble a solid line, and hence this will increase fractal dimension (top *vs.* bottom panels). If ER become spatially organized (i.e. into clumps due to stream bedform topography), as opposed to a random distribution, then larger empty spaces (i.e. pools) will occur along the line and fractal dimension will decrease (left *vs.* right panels). How fractal dimension changes with the interaction between ER number, sediment characteristics, and spatial organization is less clear.

2. Methods

We used field data from three streams each in Scotland and Australia to determine whether patterns in ER counts in 5-m segments along ~1-km stream lengths were fractal-like. We then tested the above hypotheses proposing how variables related to channel morphology and bed sediment characteristics are correlated with fractal dimensions. The Scottish and Australian sites have contrasting geomorphological histories and lithologies, and the streams vary in size and slope, so the data set captures variations in channel morphology and particle characteristics. Co-variance amongst variables used in hypothesis tests means that the empirical work is necessarily constrained.

2.1. Study systems

We investigated ER distributions from two sets of streams in SE Scotland and SE Australia (Fig. 2; Fig. 3), which have been the focus of work on insect oviposition [*Lancaster et al.*, 2010; *Reich*, 2004]. These regions have distinct bedrock geology, hydrometeorology and geomorphological histories and vary in their reach-scale channel morphology sufficient to provide a range of ER arrangements. These systems include three streams in SE Scotland (Dye Water [Dye], Faseny Water [Faseny], and Kelphope Burn [Kelphope]) and three in SE Australia (Little River [Little], Snobs Creek [Snobs], and Steavenson River [Steavenson]). The Scottish lithology is predominantly marine sedimentary (Silurian greywacke) [*Davies et al.*, 1986], whereas the Australian streams are underlain by volcanic complexes and marine sediments [*Marsden*, 1973]. The hydrology of the Scottish system is quite flashy with short-lived floods [*Lancaster*, 2000], whereas the Australian system is less so. Mean annual rainfall is ~830 mm in the area encompassing the Scottish streams (Scottish Environmental Protection Agency, https://apps.sepa.org.uk/rainfall) and exceeds 1000 mm in the Australian catchment (Australian Government Bureau of Meteorology, http://www.bom.gov.au/climate/data/). The Scottish streams in the Lammermuir Hills have a history of Pleistocene glaciation and post-glacial landscape adjustment. Each of the study reaches are located on floodplains of restricted width, set within convex hills with steep lower slopes. Intermittent coupling to hillslopes, occasional bedrock outcrops and floodplain erosion introduce some sediment to the streams but sediment supply is primarily from upstream, headwater tributaries. The Australian streams, in the Goulburn River catchment of Central Victoria, have not experienced glaciation and are set within a steeper, more mountainous landscape. The reach settings are similar to the Scottish streams, with limited floodplains, some points of hillslope coupling and occasional bedrock outcrops that affect channel orientation and recruit sediment. Woody debris is present in the Australian streams but not in the Scottish streams. Using the *Montgomery and Buffington* [1997] classification, channel morphology differs among the streams (Table S2). Dye, Faseny, and Snobs are dominated by plane bed morphology that tends toward cascades in places (steeper, smaller depth to grain size ratio) with limited true riffles. Pools between plane bed sections are common on Faseny, less common on Snobs and limited on Dye. Steavenson, Little and Kelphope comprise mostly pool-riffle morphology, most prominent in Steavenson but with increasing presence of plane bed sections in Little and Kelphope. Both regions have large variations in the proportion of pools in the study reaches (Australia: 19, 34 and 38 % of the stream length; Scotland: 14, 27 and 40 % of stream length bed (Fig. 3; Table S2). Channel width varies among the streams, from Kelphope (2.5 ± 0.5 m; mean ± SD), to Snobs (5.8 ± 1.4), Faseny (5.8 ± 1.7), Little (6.1 ± 1.7), Dye (6.6 ± 1.3), and Steavenson (9.5 ± 2.6).

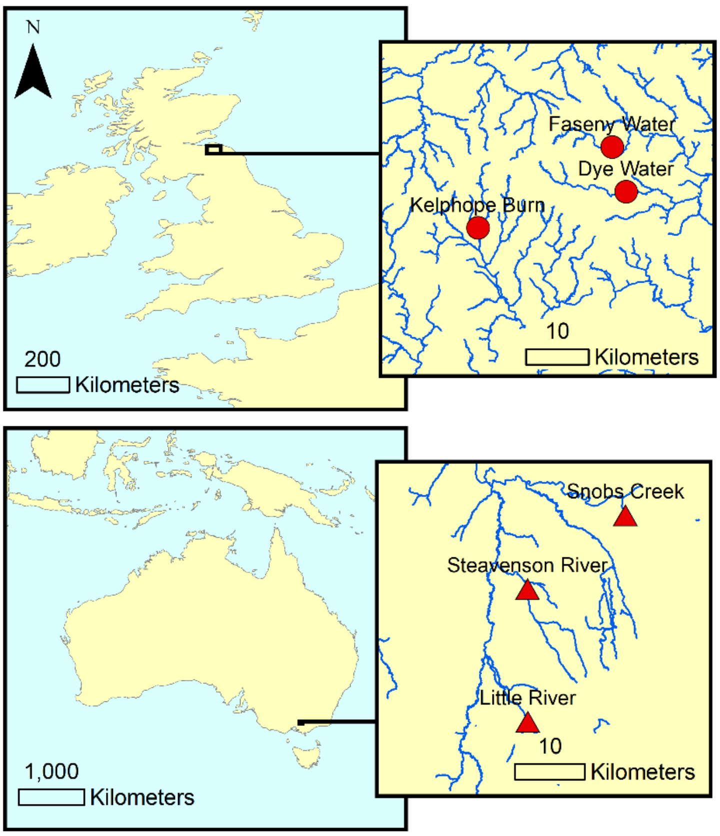

Figure 2. Scottish (circles) and Australian (triangles) study sites.

2.2. (Q1) Are longitudinal ER distributions, at scales of up to a kilometre, self-similar (fractal)?

Longitudinal profiles of ER counts were acquired to test whether patterns in ER are fractal-like and consequently whether fractal dimensions reflect geomorphological features, including measures of rock shape and channel morphology. ER of the Scottish streams were originally surveyed by *Lancaster et al.* [2010] and the Australian streams were surveyed during the Austral summer (December - February) of 2016/17. Over the study length (685 - 1000 m) of each stream, ER were counted within contiguous 5-m segments to describe the spatial distribution of patterns along the stream lengths. 5-m corresponds roughly to the average channel width of the streams. ER were defined as any rock protruding above the water surface, with a maximum b-dimension (width, perpendicular to longest axis) [*Gordon et al.*, 2004] of at least 5 cm and in at least 5 cm of water based on those typically used for oviposition by many aquatic insects. These surveys were carried out at or near summer base flow.

258 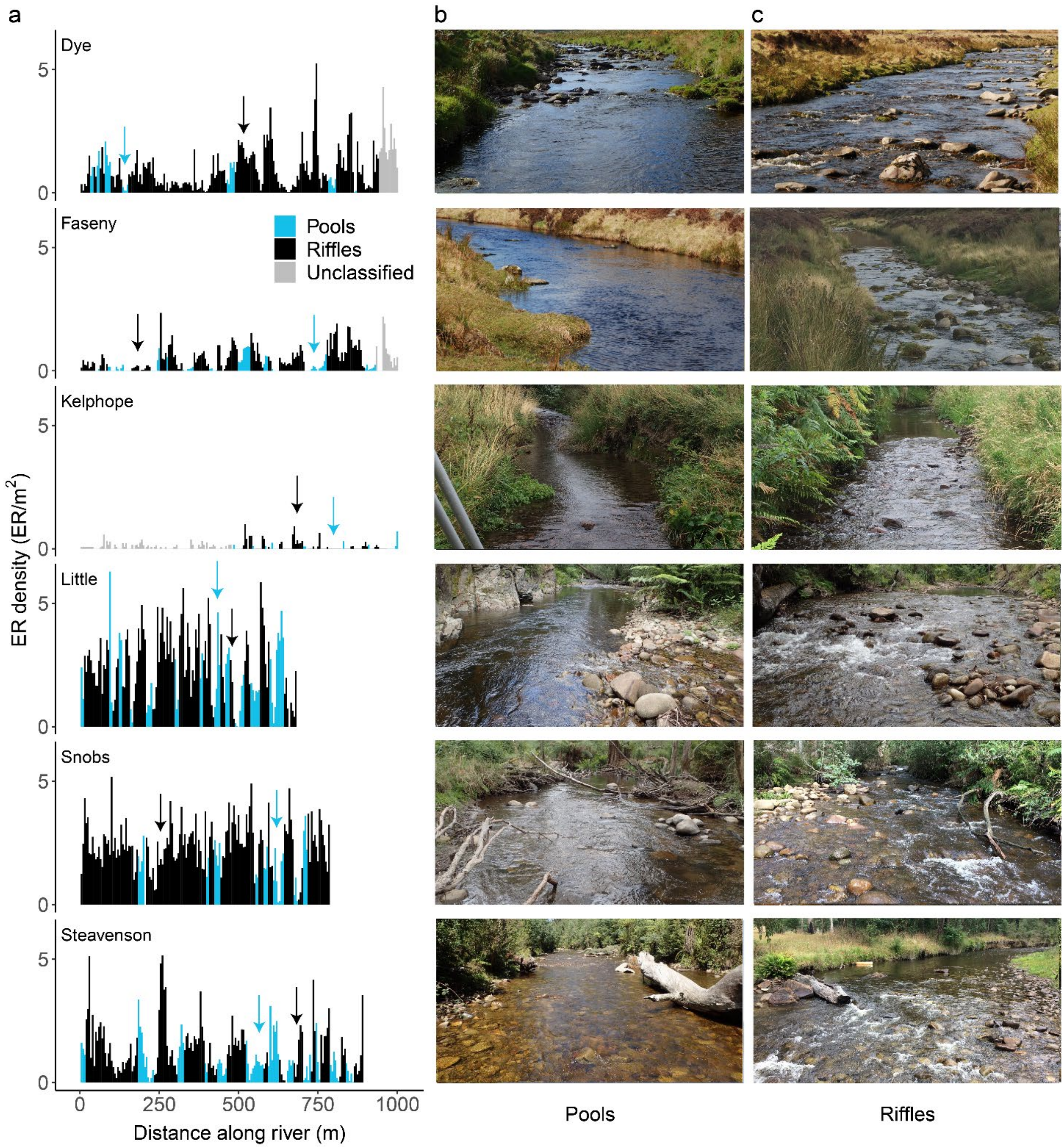

259 **Figure 3**. Longitudinal emergent rock (ER) distributions with examples of ER density in riffles and
260 pools. **(a)** Coloured bars illustrate 5-m segments denoted as pools (blue) and riffles-like segments
261 (black; inclusive of true riffles, step-pool, and plane bed; see section 2.3) for each of the six streams.
262 Unclassified segments (grey bars) were not surveyed for channel morphology. These were included in
263 the calculation of fractal dimensions but were excluded from simulations of the synthetic streams.
264 Photographs illustrate ER abundance in **(b)** pools and **(c)** riffle-like sections. Arrows indicate the
265 location of each photo.

Several methods are available for calculating fractal dimensions. Box counting is the default method, which has been used to measure complexity of forest understory and canopies [*Denny and Nielsen*, 2017], rocky shores [*Meager and Schlacher*, 2013], and aquatic plant habitat [*Ferreiro et al.*, 2011], for example. Although wide use of the box-counting method makes it well placed for comparisons among physical environments, it is a binary method calculated by counting the number of occupied boxes (N_B) and thus the underlying data are simplified to presence/absence, which results in a loss of information [*Halley et al.*, 2004]. An alternative method, the information dimension, is based on the information science parameter, entropy, and involves determining the sum of the proportion of total ER (N_E) within each box, with weighting and correction for bias [*Basharin*, 1959; *Miller*, 1955]. This method retains an estimate of the relative proportion of the variable of interest in the calculation (here ER density), thus retaining more of the underlying data and potentially providing better explanatory power for systems where relative amounts of a resource are important [*Halley et al.*, 2004]. Because entropy is not commonly used for calculating fractal dimensions, we apply both to allow comparison with other studies.

Box-counting (D_B) and entropy (D_E) fractal dimensions were calculated using methods prescribed by *Seuront* [2009]. Both methods involve dividing the stream into a set of nested equal-sized boxes, of size δ. All possible values of δ were used, i.e. 5, 10, 15, …, 1000 m, however, the data set was reduced to include only unique values of N_X (i.e. values of δ which did not result in a change in the values of N_X were excluded for either method, N_B or N_E). $\log_e(\delta)$ versus $\log_e(N_X)$ plots provide an estimate of the fractal dimensions from the absolute slope, and linearity of these plots indicates the possible presence of self-similarity (i.e. fractal structure) (Fig. 4). For our datasets, D_B will span a range of 0 (a single point) to 1 (a solid line); however, D_E retains a measure of relativity and so we might expect values greater than 1.

To avoid making assumptions of linearity in the log-log plots, we followed *Seuront's* [2009] three-step procedure to detect fractal-like properties in natural patterns. This ensures that only patterns that are fractal are described as such. These steps included the: 1) R^2 – SSR [sum of squared residuals] Procedure, 2) the Zero-Slope Procedure and 3) the Compensated-Slope Procedure. *Seuront* [2009] specified that data sets could be considered fractal-like if they satisfied any two criteria of the three-step procedure. Reported estimates of the fractal dimensions (D_X; unspecified method) in the results were taken from the Compensated-Slope

Procedure because this estimate is more robust to random non-fractal structure (i.e. artefacts of the data). All computations were undertaken using packages ggpmisc, stats, lmodel2 and plyr in the open-source software R [*R Core Team*, 2019]. A more detailed description of calculating fractal dimensions using *Seuront's* [2009] three-step procedure (Text S1; Fig. S1) and the corresponding R script (Script S1) can be found in Supporting Information.

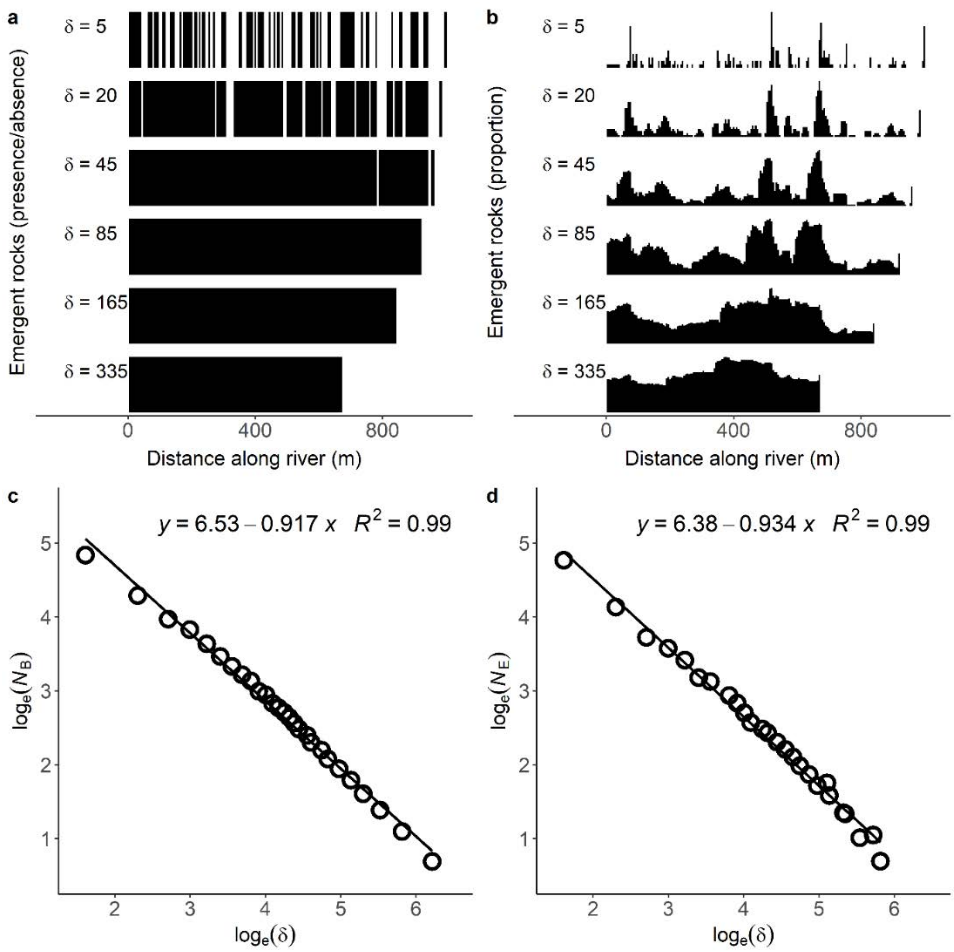

Figure 4. Calculating fractal dimensions of emergent rock (ER) distributions. To calculate fractal dimensions, longitudinal counts of ER in 5-m segments along a 1-km stream stretch are observed at different box sizes (δ). The minimum box size in fractal dimensions calculations corresponds to the 5-m segments ($\delta = 5$). The box-counting fractal dimension (D_B) and the entropy fractal dimension (D_E) methods use the presence **(a)** or proportion **(b)** of ER in each box, respectively. For all possible box sizes (only six values of δ are illustrated), the box-counting method calculates N_B from the sum of boxes containing ER, whereas the entropy method calculates N_E from the sum of the proportions of ER within each box. Significant linearity in $\log(N_B)$ **(c)** and $\log(N_E)$ **(d)** plots with changing $\log(\delta)$ indicates the possible presence of a fractal structure. The absolute slope of this line can be used as an

estimate of fractal dimension (here, D_B and D_E are 0.917 and 0.934, respectively). Equations are expressed in log-transformed units.

2.3. (Q2) Do fractal dimensions capture differences in ER distributions between rivers associated with differences in channel morphology and sediment characteristics?

As we confirm below, all six rivers are self-similar, which means their fractal dimensions capture scale-independent aspects of how ER are distributed in these streams. Next, we tested how fractal dimensions of ER vary with geomorphological variables related to bed topography, because this affects the propensity of ER to be emergent and structured in space (e.g. the strength of alternating pool-riffle development), and with the size and shape of bed materials, because these affect the abundance of ER (Fig. 1). We conducted surveys to provide measures of these characteristics.

Channel morphology surveys were carried out in Sept. 2018 in Scotland and Feb. 2018 in Australia when discharge was at or near summer base flow. Surveys of morphology and ER were aligned to ensure spatial compatibility. Morphological surveys were carried out on a reduced section of the ER survey length (525 – 940 m; Fig. 3), which was visually classified for morphology at 2-3 m intervals using *Montgomery and Buffington* [1997] typology, as described above and in Table S2. The primary purpose was to characterise the distribution and arrangement of morphological units that are more or less likely to contain ER. We therefore used a simplified binary morphological classification of pools and 'riffle-like', lumping together true riffles, plane beds and step-pools as sections where the flow is relatively shallow and bed materials are more likely to be exposed. For simplicity, we refer to these sections as riffles and pools hereafter.

To document bed and water surface topography, a longitudinal survey was completed using a dumpy level, with measurements at each interval along the thalweg. Channel width was measured during the ER surveys at intervals of every 10 m for Scottish streams and every 20 m for Australian streams. The latter were measured at a coarser scale due to an observed lack in variance. The shape and size of ER and submerged rocks were also surveyed. Dimensions of ER and submerged rocks were measured at the top, middle and bottom of the survey length using Wolman counts of 100 rocks at each location [*Wolman*, 1954]. We measured a (length), b (width), and c-axes (thickness) of each rock to the nearest 5 mm [*Gordon et al.*, 2004; *Rice and Church*, 1996]. We characterised both ER and a random sample of submerged rocks to determine whether the attributes of the ER themselves (which were used to calculate the fractal dimensions) or the characteristics of the available bed materials, which are better represented by the submerged rocks, are related to fractal dimensions.

Given the exploratory nature of the work, we calculated a suite of relevant variables from these field data (Table S1; Table S3) and tested for correlation with fractal dimensions. For morphology, variables included stream slope, mean riffle and pool lengths (calculated relative to the study length) and the number of pool-riffle transitions. For grain size we used the mean of b and c axis and for shape we calculated mean values of equancy (c-axis/a-axis) and flatness (c-axis/b-axis) ratios [*Blott and Pye,* 2008]. Some of these measures were correlated with each other, particularly measures of sediment size and shape (Table S4). Moreover, the expectation of finding more ER in riffles than pools simplifies what is often a complex pattern and is probably unrealistic in some streams. Our field observations confirmed that, on average, riffles contained more ER than pools but also that most pools also contained some ER in varying amounts. We therefore included several additional metrics (Table S3) in the correlation tests that were intended to accommodate some of this uncertainty. First, we calculated the mean ER density in each study reach to capture differences in the relative abundance of ER between the streams. Second, we removed stream morphology altogether by dividing the reaches into sections with and without ER and calculating metrics for those units, including the number of segments without ER (Table S3). These allow us to ask the fundamental question of whether fractal dimensions are related to patterns of ER presence and absence, irrespective of whether that presence or absence is related to the pools and riffles identified in the field surveys.

Correlation tests (Pearson's product moment coefficient) were used to determine whether fractal dimension is able to capture between-stream differences in ER associated with differences in channel morphology and sediment characteristics, differences in the density of ER in pools and riffles, and differences in the pattern of reaches with and without ER. These were one-tailed correlation tests because, as explained in the Introduction, fractal dimension can only increase with numbers of ER, and can only decrease with an increase in the spatial structure of ER. Relationships in the opposite directions are either mathematically impossible, or at least improbable for the range of variable values likely to be encountered for ER in rivers.

2.4. *(Q3) Using synthetic streams, which aspects of stream morphology are responsible for driving differences in fractal properties?*

Multiple variables affecting fractal dimension were correlated with each other, hence we created synthetic streams in a numerical model. These synthetic streams allowed some stream characteristics to be manipulated individually and with greater replication, to test how the characteristics influence fractal dimensions. Simulations were carried out in R based on empirical measurements of morphological characteristics and ER numbers (for example see Supporting Information Fig. S3), although some empirical data could not be simulated (e.g. rock shape and size). Synthetic stream stretches were created by first randomly drawing riffle and pool lengths from log-normal distributions. Riffle and pool lengths were alternated for the length of the synthetic stream (1000 m). ER counts were then randomly drawn from the negative-binomial distributions and assigned to each 5-m segment of the riffle and pool lengths. Log-normal distributions of riffle and pool lengths were produced from the observed lengths of pools and riffles, which were fit to separate log-normal distributions. Log-normal distributions were chosen because riffle and pool lengths are continuous, positive (> 0) and skewed with few high values. ER counts in riffle and pool segments were fit to separate negative-binomial distributions. Negative-binomial distributions were chosen because these data are discrete, nonnegative (≥ 0), and skewed (i.e. suitable for few high ER counts). As the ER distributions of the study streams fell into two distinct groups (those with few *vs.* many segments without ER), separate negative-binomial distributions were produced from these two groups to capture these differences (see Supporting Information Text S2 and Fig. S2 for illustration). Low-zero streams (few segments containing zero ER) were simulated from the ER count distributions of Dye, Little, Snobs, and Steavenson. High-zero streams (many segments containing zero ER) were simulated from the ER count distributions of Faseny and Kelphope.

To determine the effect of stream characteristics on fractal dimension, pool length, riffle length, and ER density were varied either individually or in combination and replicated 20 times. To disentangle the pattern of segments without ER from the total number of segments without ER, an additional set of synthetic streams was produced by alternating riffles with ER (randomly drawn from the negative-binomial distributions) and pools without ER of the same lengths. The lengths of the riffles and pools were not drawn using random processes but were systematically set to 14 different lengths, including: 5 (every second 5-m segment has no ER), 10 (two 5-m segments with ER, two 5-m segments without ER), 25, 50, 75, 100, 150, 200, 250, 300, 350, 400, 450, and 500 m. For lengths that are factors of 1000 (the length of the stream), the pattern of segments without ER will change, but the number of segments without ER remains constant at 100 [500 m]. Twenty replicate synthetic streams were produced for each of the 14 riffles and pool lengths. A total of 1360 synthetic streams were simulated using both the random and systematic processes. For a more detailed description of these simulations and the R script, see Supporting Information Text S2 and Script S2, respectively. As a first test to see whether the ER distributions of low and high zero synthetic streams produced systematically different values of D_E, t-tests were used. To test for differences in the variation of D_E and variation in the number of ER between the two distributions, modified signed-likelihood ratio (M-SLR) tests were used [*Krishnamoorthy and Lee*, 2014]. M-SLR tests were implemented using the R package CVEQUALITY [*Marwick and Krishnamoorthy*, 2018]. Two-tailed linear regression analyses were performed to test for relations between fractal dimensions and channel morphology characteristics. The slopes of lines show not only the direction of relationship with fractal dimension but also the relative effect of each independent variable; steep slopes signal greater change in fractal dimension than shallow slopes.

3. Results

3.1. (Q1) Are longitudinal ER distributions, at scales of up to a kilometre, self-similar (fractal)?

The ER distributions of all six streams were fractal-like using both the box-counting and entropy methods. All streams satisfied at least two of the three tests developed by *Seuront* [2009]; this is sufficient to illustrate fractal behaviour (Table S5). Further, coefficients of determination for all streams ranged from 0.99 to 1.0 for both the box counting and entropy fractal dimensions (Fig S4). Fractal dimensions varied among the six streams and with the method of calculation (Fig. 5). There was very little discrimination among the streams using the box-counting method (Table S5; Fig. 5a): four streams (Steavenson, Dye, Snobs and Little) had the same value for D_B and this value did not differ from the fractal dimension of a straight line (1.00), because very few segments (≤ 2; equivalent to ≤ 10 m) in these streams contained zero ER. Of the remaining streams, D_B was 0.97 for Faseny (although statistically the log-log slope was not significantly different from 1; Fig. S4) and 0.90 for Kelphope. Significant breaks in the box-counting log-log slopes were found for all streams except Snobs and Steavenson (Fig. S5).

The entropy fractal dimension (D_E) largely matched the rank order of streams using the box-counting method, but it discriminated numerically between all six streams. Values of D_E ranged from 0.91 to 1.05 and the rank order of streams from lowest to highest D_E was Kelphope (0.91), Faseny (0.93), Steavenson (0.98), Dye (1.00), Little (1.02), and Snobs (1.05) (Fig. 4b). This produced two groups, whereby log-log slopes for Kelphope and Faseny were significantly different from that of Steavenson, Little and Snobs (Fig. S4). Dye was only significantly different to Kelphope. The log-log slopes for all streams except Dye were significantly different from 1 (Fig. S4). Significant breaks in log-log slopes were found for all streams, the position of these varied among the streams and was significantly correlated with pool length and pool-riffle ER density ratio (Fig. S5). Due to its superior ability to differentiate among streams, we consider D_E the better method of measuring the complexity of ER distributions in our six streams. Therefore, analysis for questions Q2 and Q3 used only the entropy fractal dimension (box-counting results can be found in Supporting Information Table S6, Table S7 and Table S8).

3.2. (Q2) Do fractal dimensions capture differences in ER distributions between rivers associated with differences in channel morphology and sediment characteristics?

Entropy fractal dimensions correlated well with some stream characteristics. D_E was negatively correlated with three stream characteristics that relate to the spatial arrangement of ER: mean proportional pool length, the number of segments without ER and the maximum length without ER (Table 1). D_E was positively correlated with slope and ER density, which relate to the number of ER. D_E was also positively related to sediment characteristics of submerged rocks: the c-axis length, and equancy ratio. Given the small sample size (n = 6), these results should be interpreted with caution given prospective lack of statistical power for some tests. More critically, some of the independent measures of stream characteristics are correlated with each other, as well as with fractal dimension, which creates uncertainty about cause and effect (Supporting Information Table S4).

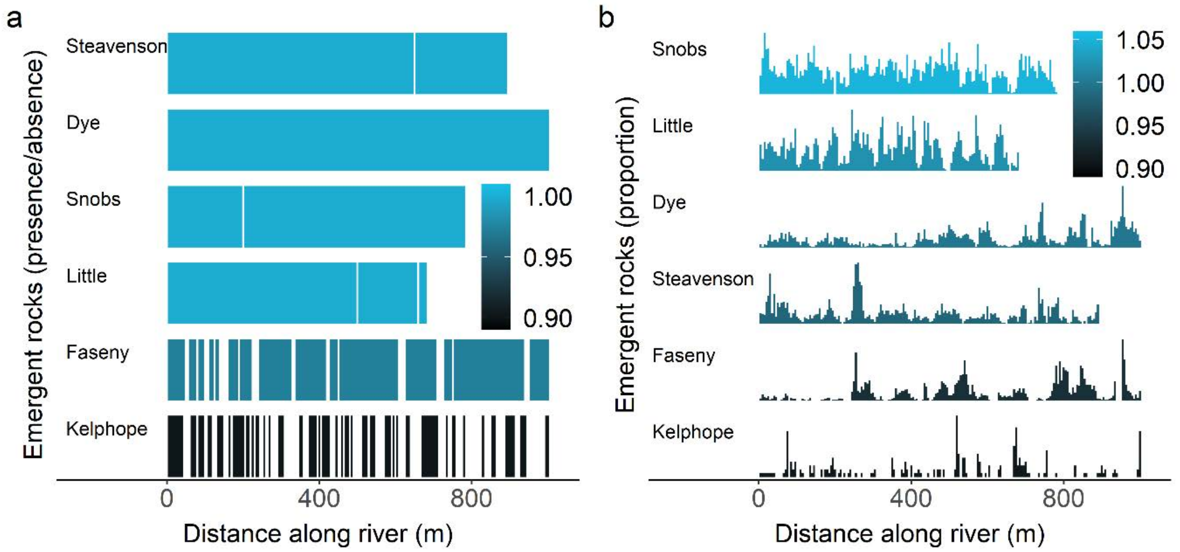

Figure 5. Fractal dimensions of emergent rock (ER) distributions. ER distributions along stretches of three Australian streams (Little; Snobs; and Steavenson) and three Scottish streams (Dye; Faseny; and Kelphope). Bars represent the presence (a) or proportion (b) of ER in each 5-m segment (the minimum box size used in fractal dimensions calculations) and fill colour and the order of the streams reflects the box counting fractal dimensions (DB for a) or the entropy fractal dimensions (DE for b) of the ER distributions.

Table 1. Study streams: Correlation tests (one-tailed) of associations between various stream characteristics and entropy fractal dimensions.

Characteristic	**Expected direction**	**r**	**p**
Stream morphology			
Median depth	Negative	0.791	0.969
Stream slope	**Positive**	**0.737**	**0.047**
Mean proportional pool length	**Negative**	**-0.870**	**0.012**
Mean proportional riffle length	Positive	0.054	0.460
Number of pool-riffle transitions	Negative	0.241	0.677
Bed sediment			
SR (submerged rock) axis B	Positive	0.653	0.080
SR axis C	**Positive**	**0.950**	**0.002**
SR equancy ratio (C/A)	**Positive**	**0.765**	**0.038**
SR flatness ratio (C/B)	Negative	0.755	0.958
ER density measures			
Mean ER density over entire site	**Positive**	**0.917**	**0.005**
Pool-riffle ER density ratio	Negative	0.541	0.866
Segments without ER			
Number of segments without ER	**Negative**	**-0.832**	**0.020**
Maximum length without ER	**Negative**	**-0.895**	**0.008**

Note. Bold text indicates $p < 0.05$ in the direction expected for the one-tailed correlation tests; DF = 4 for all tests. Tests involving sediment size and shape of ER were all non-significant and are reported in Table S6.

Table 2. Synthetic streams: Linear regression tests (two-tailed) for relationships between various stream characteristics and entropy fractal dimensions, for low-zero streams (LZS) and high-zero streams (HZS) in different simulations. For each simulation pool and riffle lengths, and the number of ER in pools and riffle segments were held constant except for the manipulated variables.

Independent variable	Manipulated variable(s)	ER dist.	DF	Slope	t	p	R^2	Fig.
Stream morphology								
Mean proportional pool length	Pool lengths	LZS	78	**-8.9×10^{-5}**	**3.48**	**<0.001**	**0.13**	7b
		HZS	78	**-7.8×10^{-4}**	**4.84**	**<0.001**	**0.23**	
Mean proportional pool length	Pool lengths, riffle ER	LZS	77	**-3.8×10^{-3}**	**15.5**	**<0.001**	**0.76**	7d
		HZS	77	**-4.6×10^{-3}**	**8.46**	**<0.001**	**0.48**	
Mean proportional riffle length	Riffle lengths	LZS	77	8.2×10^{-6}	0.88	0.38	<0.01	NA
		HZS	77	1.3×10^{-6}	1.88	0.06	0.04	
ER density measures								
ER density	Riffle ER, pool ER	LZS	78	-1.3×10^{-6}	0.70	0.49	<0.01	NA
		HZS	78	7.1×10^{-5}	0.83	0.41	<0.01	
Mean density of riffle ER	Riffle ER	LZS	78	**-1.1×10^{-4}**	**12.3**	**<0.001**	**0.66**	7a
		HZS	78	**-4.2×10^{-4}**	**5.02**	**<0.001**	**0.24**	
Mean density of riffle ER	Pool lengths, riffle ER	LZS	77	**-3.2×10^{-4}**	**22.4**	**<0.001**	**0.87**	7c
		HZS	77	**-1.9×10^{-3}**	**17.1**	**<0.001**	**0.79**	
Pool-riffle ER density ratio	Riffle ER	LZS	78	**0.075**	**11.9**	**<0.001**	**0.64**	NA
		HZS	78	**0.093**	**4.97**	**<0.001**	**0.24**	
Pool-riffle ER density ratio	Pool lengths, riffle ER	LZS	77	**0.19**	**13.3**	**<0.001**	**0.69**	NA
		HZS	77	**0.38**	**9.71**	**<0.001**	**0.55**	
Segments without ER								
Number of segments without ER	Pool lengths	HZS	78	**-1.2×10^{-3}**	**6.18**	**<0.001**	**0.33**	6a
Maximum length without ER	Pool lengths	HZS	78	-1.8×10^{-3}	1.29	0.20	0.02	6b
Number of segments without ER	All*	LZS	278	**-3.1×10^{-3}**	**7.91**	**<0.001**	**0.18**	6c
		HZS	278	**-3.9×10^{-3}**	**9.12**	**<0.001**	**0.23**	

Note. t-tests indicate whether slopes differ from zero, significant tests are shown in bold text. See supporting material for full description of simulations. *Alternating riffles with ER (randomly drawn from the negative-binomial distributions) and pools without ER of the same lengths.

3.3. (Q3) Using synthetic streams, which aspects of stream morphology are responsible for driving differences in fractal properties?

Consistent with the study streams, D_E of synthetic stream stretches was associated with stream characteristics that relate to the spatial arrangement of ER, namely the number of segments without ER, the maximum length without ER, and pool length. Without manipulating stream characteristics (pool length, riffle length, or ER density), D_E was significantly different for simulations using the two ER distributions, i.e. low *vs.* high zero streams ($t = 34.2$, $p < 0.001$). This suggests that the number of segments without ER influence D_E, however the number of ER in pools and riffles could also contribute to this result. Variation in D_E was significantly larger for the high-zero streams (Mean $D_E \pm$ SD; 0.93 ± 0.012) compared with the low-zero streams (1.02 ± 0.002; M-SLR = 39.03, $p < 0.001$). By definition the number of segments without ER and the maximum length without ER differed between the two ER distributions. However, as these simulations mimic the natural systems, they also differed significantly in ER density ($t = 69.8$, $p < 0.001$) and variance (M-SLR = 9.13, $p = 0.003$). Interestingly, the difference in ER variance was in the reverse direction to the variation in D_E, with the low-zero streams having higher ER variance (Mean ER/m $\pm$ SD; 10.90 ± 0.51) than the high-zero streams (1.94 ± 0.26). D_E of simulated stream stretches was also negatively associated with the number of segments without ER for high-zero streams with pool lengths manipulated to influence the number of segments without ER (Table 2, Fig. 6a). The maximum length of segments without ER was not related to D_E for these simulations (Table 2, Fig. 6b), which contradicts the results from the study streams. However, systematic introduction of pools without ER resulted in a clear non-linear pattern of D_E with the maximum length of segments without ER (Fig. 6d). For these simulations, minimum D_E resulted from pools (and riffles) of 50 – 75 m (10-15 segments) in length and maximum D_E was observed with pools of 350 m (70 segments) in length. D_E was also negatively associated with the length of pools, even when almost all segments contained ER, as seen by manipulating pool length of low-zero streams (Table 2). The same trend was seen for high-zero streams however, this increased pool length and the number of segments without ER concurrently.

Relating to the number of ER, only ER density could be manipulated in simulations to create certainty about cause and effect, whereas depth, slope and sediment characteristics could not be simulated. Unlike the study streams, D_E was not correlated to overall ER density of simulated stream stretches, as tested by manipulating the number of ER in pools and riffles in combination (Table 2; Fig. 7). D_E decreased with ER density when only the number of ER in riffles was manipulated (Table 2; Fig. 7a), however this negative relationship conflicts with our expectations and the results from the study streams. This manipulation concurrently created a gradient in the pool-riffle ER density ratio, which may have produced the unexpected relationship. This is supported as further exaggeration of pool-riffle structure by manipulations of ER density and pool length together, such that the highest ER densities were paired with the longest pools creating the strongest relative difference (Fig 5c, d), increased the magnitude of the slopes of D_E for both high-zero streams and low-zero streams. Taken together, these results demonstrate that the spatial arrangement of ER (pool/riffle structure) has a stronger effect on D_E than ER density.

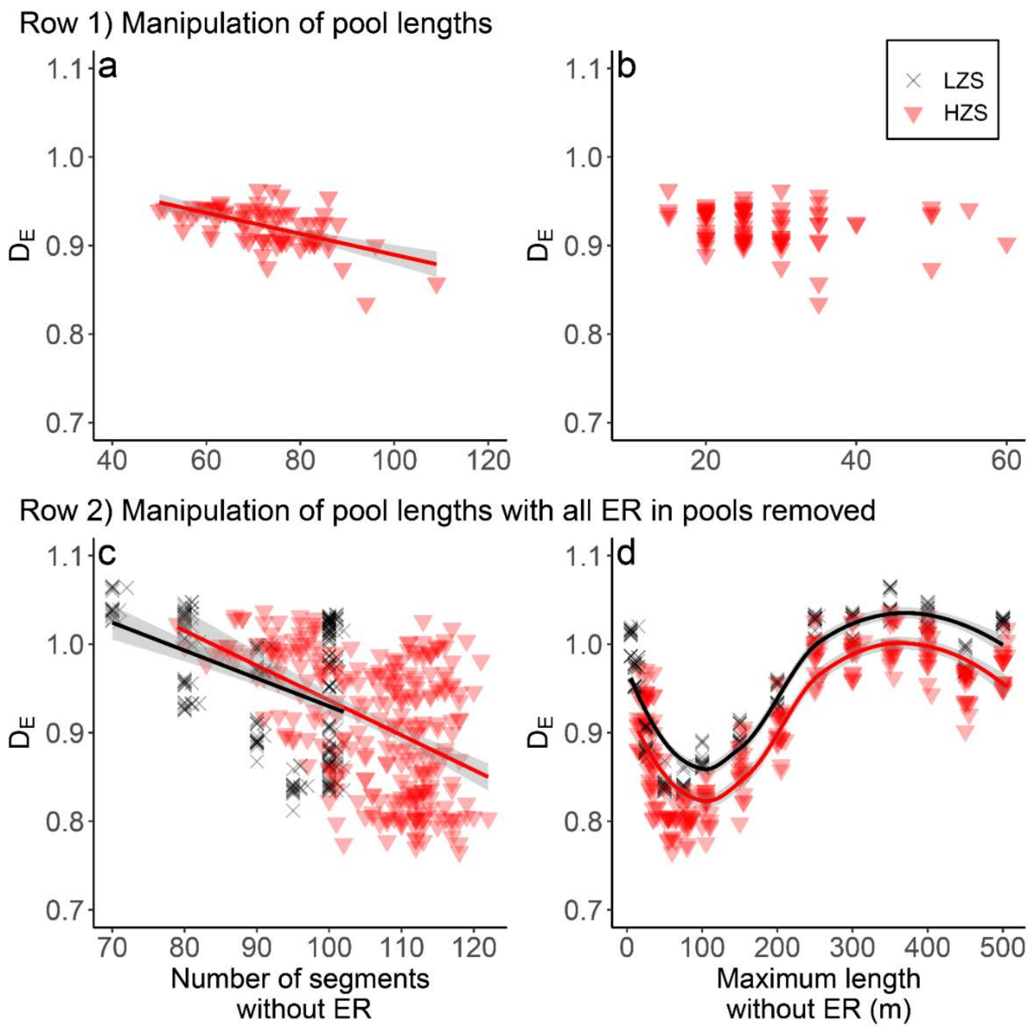

Figure 6. Using synthetic stream stretches to determine the influence of segments without ER on D_E. **(a-b)** The number of segments without ER was altered by manipulating pool lengths of high-zero streams (HZS: red triangles). D_E was associated with the number of segments without ER **(a)** but not the maximum length of segments without ER **(b)**. Low-zero streams (LZS) were not included in this analysis as increasing pool lengths did not largely influence the number of segments without ER. **(c-d)** Further simulations whereby segments without ER were included by alternating pools without ER and riffles with ER (using LZS (grey crosses) and HZS riffle distributions) for the length of the site (1000 m). Pools and riffles were of length 5 (every second 5-m segment has no ER), 10 (two 5-m segments with ER, two 5-m segments without ER), 25, 50, 75, 100, 150, 200, 250, 300, 350, 400, 450, and 500 m. In accord with the first set of simulations, increasing the number of segments without ER resulted in a linear decline in D_E **(c)**, however, the length of segments without ER resulted in a clear non-linear relationship with D_E **(d)**. Loess curves are fit to non-linear relationships to illustrate patterns. See Table 2 for summary of statistical tests.

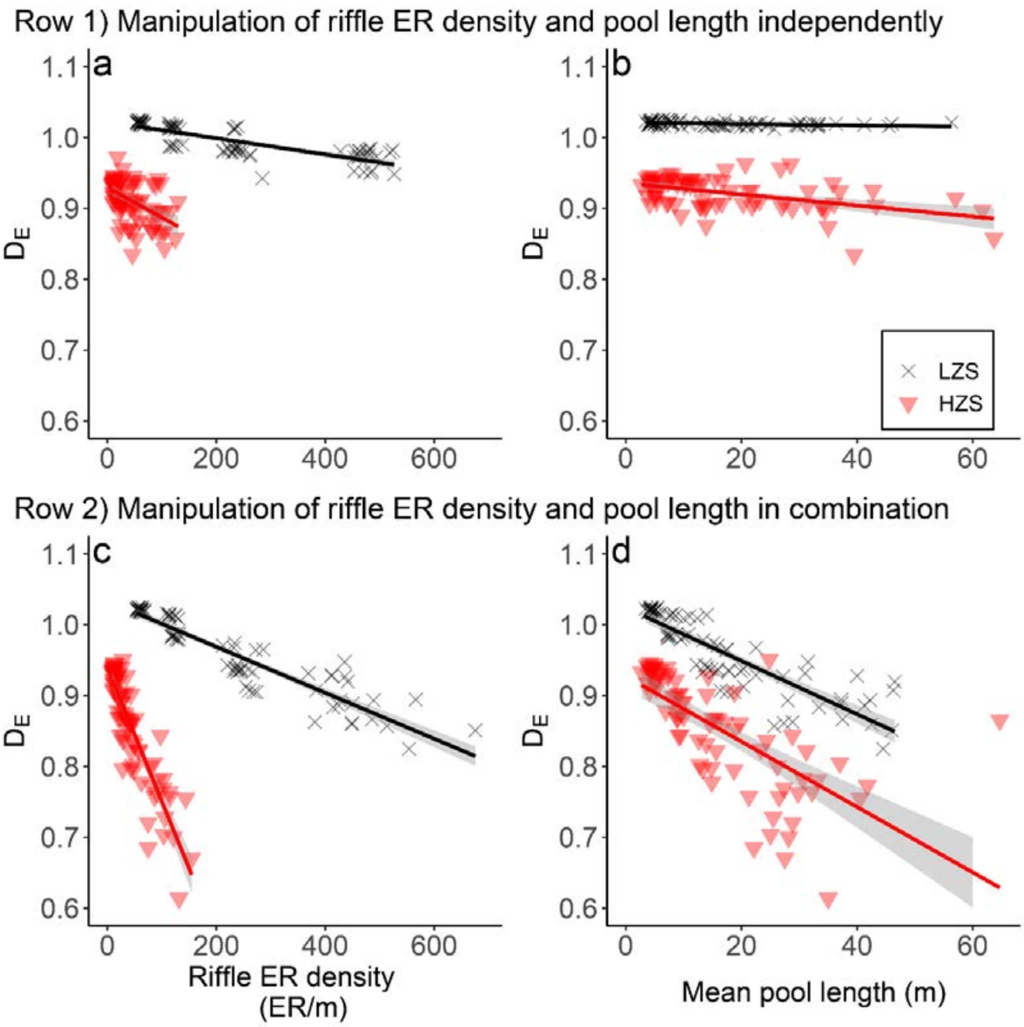

Figure 7. Using synthetic stream stretches to determine the influence of pool-riffle structure on entropy (D_E). D_E is influenced by pool-riffle structure when described by the relative difference in ER density between pools and riffles and the relative length of pools and riffles. Simulations used the two ER distributions: low-zero streams, LZS (grey crosses) and high-zero streams, HZS (red triangles) with manipulations of **(a)** ER density in riffles *or* **(b)** pool length, independently of each other, *or* **(c-d)** both ER density in riffles and pool length *in combination* (i.e. panels **c** and **d** are drawn from a single set of simulations). ER density in riffles and pool length independently influenced LZS and HZS simulations, however a greater effect (steeper slope) occurred when both stream characteristics were manipulated. See Table 2 for summary of statistical tests.

4. Discussion

4.1. (Q1) Are longitudinal ER distributions, at scales of up to a kilometre, self-similar (fractal)?

Fractal dimensions can be used to measure the complexity of ER distributions in streams in a way that is scale independent. Six streams exhibited fractal behaviour (self-similarity) according to the criteria developed by *Seuront* [2009] for both the box-counting and entropy methods. It seems likely that fractal dimensions may also measure complexity at scales smaller than the reach (e.g. single riffles) and beyond our reach lengths (regional scales). However, we provide some evidence that our study streams exhibit multiple scaling behaviour as discerned by breaks in the slope of the log-log plots, which may indicate that different scaling regions (ranges of δ) are described by different fractal dimensions. The position of the breaks varied among the streams and could be associated with the scale of bedform spacing (Figure S5). This could also be an artifact of reaching the limits of the data sets, and so further exploration is needed to determine whether a single or multiple relationship is better linked to channel geomorphology. Because at least three orders of magnitude are recommended for fractal analysis [*Falconer*, 1993] and our datasets confirm fractal behaviour, even when these breakpoints are crossed, we will continue the discussion with the box-counting and entropy fractal dimensions calculated using the entire dataset to ensure the relevance of the fractal analysis.

Fractal dimensions varied among the six streams and with the method of calculation. The box-counting method only differentiated between streams with many (1 stream), few (1 stream) and no (4 streams) segments without ER. This is problematic for comparison of upland streams where the vast majority of segments in streams have at least one ER, which results in $D_B \sim 1$ (the value for a straight line). With a higher resolution, the entropy method separated all six streams, indicating that the arrangement of ER varies among the streams. D_E ranged from 0.91 to 1.05, and while this is likely a narrow distribution out of a greater range of fractal dimensions that are possible for real rivers, this range provides some opportunity to relate ER arrangement to channel morphology and sediment characteristics using the study streams. However, multicollinearity in the natural systems necessitates the use of synthetic streams to isolate the causes of variation in D_E among streams.

4.2. (Q2) Do fractal dimensions capture differences in ER distributions between rivers associated with differences in channel morphology and sediment characteristics?

Our field data showed that entropy fractal dimensions correlated well with stream characteristics that relate to the number and spatial arrangement of ER. Concerning the number of ER, D_E was related to ER density and channel morphology and sediment characteristics that influence the propensity for large rocks to emerge. As expected, D_E was positively correlated with the c-axis and particle equancy (c/a) of the bed materials, as characterised by random sampling of submerged sediments. Submerged rocks likely provide a better characterization of the bed materials than ER (which were not correlated with D_E), which capture only a subset of the sediment distribution. At a given water depth, grains that have a large c-axis and are more equant are more likely to be emergent because most grains rest on their a-b plane, so that the c-axis then determines the elevation of the upper surface of the particle. Notwithstanding differences in water depth between streams, larger mean c-axis and equancy are therefore likely to increase the abundance of ER. Indeed, our data showed a significant positive correlation of both c-axis and particle equancy with ER density. This suggests that rock shape may influence the likelihood of emergence more than size (b-axis was not correlated with D_E). However, there is also an expectation that c-axis varies with channel slope, such that larger bed materials are more common in steeper channels (because slope is generally adjusted to generate shear sufficient to transport the coarsest materials) and that as channel length (or drainage area) increases, so the maximum particle size declines due to sorting and abrasion processes. As slope also influences bedform development causation may be linked more closely to the spatial arrangement of ER.

Our expectation that the fractal dimension would be related to the spatial arrangement of ER was supported by stream characteristics that identify the presence of pool and riffle structure. These included negative correlations of D_E with the number and maximum length of segments without ER, mean proportional pool length, and slope. Segments without ER provide the first evidence of pool-riffle structure however, at this coarse scale, pools are simplified to segments without ER, which rarely occurs. At a finer scale, all streams showed some degree of pool-riffle structure, with riffles in each stream having higher ER density compared to pools. This structure was greater for three streams (Kelphope, Faseny, and Steavenson) where pools had fewer than half as many ER as riffles (<0.5:1; pool:riffle ER ratio); this resulted in the lowest values for D_E. Accordingly, these streams have well-developed macro-scale bedforms like alternating pools and true riffles (e.g. Steavenson) or alternating pools and plane bed sections (e.g. Faseny). For the remaining streams (Snobs, Little and Dye), the ratio of ER in pools and riffles was less pronounced (>0.7:1) and led to the highest values of D_E. Topographic bedform development is weak in these streams (e.g. Dye and Snobs), and hence there is more chaotic, limited organisation of ER. In reaches dominated by plane bed or with weak riffle-pool development, an absence of long pools suggests that sediment storage dominates throughout, with little longitudinal topography. This storage of sediment uniformly elevates the bed closer to the water surface and there is a greater chance of rocks emerging. In contrast, where storage is organised into distinctive topographic highs and lows, the propensity for large rocks to emerge is alternately higher and lower. It is also notable that the steepest streams in each region (Dye, Snobs) are those with the more irregular ER distributions whereas those on lower slopes (Faseny, Little, Steavenson) have better developed bedforms and ER organisation. This reflects the well-known association between channel steepness and bedform type, with the development of true riffle and pool sequences on slopes typically below 1 % [e.g. *Buffington and Montgomery*, 2013].

The study streams provide evidence that larger, more-equant grain sizes are associated with greater abundance but weaker longitudinal organisation of ER. This reinforces the suggestion that steeper, and also smaller catchments, are more likely to be associated with high D_E. This study is the first to investigate the fractal behaviour of ER in streams and so comparisons with previous studies are limited; however, relationships with catchment characteristics align with previous work on fractal dimensions of river networks, which are related to runoff and sediment yield [*Yang and Shi*, 2017], flood frequency [*Zhang et al.*, 2015], climate [*Wang et al.*, 2009], and tectonic forces [*Shen et al.*, 2011]. Ultimately, the number of emergent rocks and the presence of well-developed topographic bedforms reflects the interplay of many underlying geomorphological processes. This creates difficulties when attempting to identify relationships between those variables and other constructs, such as fractal dimension, because variables are not independent and mechanisms are difficult to disentangle. Simulating streams provides an elegant way to address these issues.

4.3. (Q3) Using synthetic streams, which aspects of stream morphology are responsible for driving differences in fractal properties?

The simulated synthetic streams provided a clear basis upon which to hypothesise mechanisms that underpin the relationship between any individual measure of stream morphology and fractal dimension. They revealed a clear relationship of decreasing fractal dimensions, and therefore stronger longitudinal organisation of ER, with increased pool-riffle structure (Fig. 7). To illustrate this clearly, pool-riffle structure was exaggerated by increasing pool lengths, the number of segments without ER in pools, and ER density in riffles relative to pools (each manipulated independently from each other and in combination). The strongest effects were seen when these characteristics were manipulated in combination, and changes were greater than the sum of the individual effects. This shows that fractal dimensions capture the dynamics of multiple characteristics making them more useful than measuring any single characteristic. The use of simulations to investigate these dynamics allows unhindered interpretation of results and have provided clear complementary support for the arguments made using the empirical analysis for a relationship between pool-riffle structure and fractal dimension in the study streams.

Taken together, the field and simulated components of this study have helped to disentangle the geomorphological processes that may generate variation in physical complexity. Fractal dimensions captured well-known patterns that arise from sediment sorting, abrasion, and storage processes and are associated with longitudinal fluvial gradients. Upstream, steeper slopes, less well-developed bedform topography, and greater abundances of large rocks lead to an irregular organisation of ER and high fractal dimension. Downstream, the development of true riffle and pool sequences on low slopes and lower abundances of large rocks result in stronger longitudinal organisation of ER and low fractal dimension. Variation in D_E values between streams relates to aspects of stream morphology and sediment character. As such, the entropy fractal dimension is a promising measure of physical complexity that captures differences in ER distributions and organisation driven by geomorphological processes. D_E is, therefore, a useful metric in both geomorphological and ecological studies, which frequently rely on measurements of geomorphological characteristics to explain ecological patterns.

4.4. Fractal dimensions across ecosystems

Landscape complexity generates patchiness in environmental conditions (e.g. flow resistance, turbulence, etc.) and resources (e.g. living spaces and food) that drive ecological processes

[*Huffaker*, 1958]. This patchiness can facilitate or impede dispersal of organisms, abundance and persistence of species, and interactions among species. Entropy, describing the complexity of the physical landscape, is likely to be related to these ecological processes with the added benefit of being comparable across disciplines and potentially across subject matter. The entropy fractal dimension may therefore be useful for bridging the gap between ecology and geomorphology, enabling general questions of assembly to be tested across ecosystem types.

Self-similarity allows fractal dimension metrics to be transferred across ecosystem types even when they are measured at different scales. While we have shown that the entropy fractal dimension may be a useful method to describe the landscape complexity of streams, the box-counting method is still more commonly used across many disciplines. Using a common method allows integration of ecosystem patterns and broad-scale hypotheses tests across landscapes scales, and so corresponding results using box counting are presented in the Supporting information (Table S6, Table S7 and Table S8). While integrating patterns among ecosystems was not the purpose of this study, it is interesting to note that the complexity and lack of structure of ER habitats (D_B = 0.92 - 1.00) seen here is generally greater than that reported for other systems where D has been measured in one dimension, including evergreen forest canopy (0.78 - 0.95), deciduous forest canopy (0.69 - 0.95), understory shrubs (0.70 - 0.81), grassland shrubs (0.61) and grassland grasses (0.80) [*Denny and Nielsen*, 2017; *Ritchie*, 2009] (slopes of log-log plots are reported here to provide consistency with other papers). How this relates to ecological response variables in these habitats (i.e. species diversity, dispersal) is an interesting avenue for further research. Ultimately, determining whether fractal dimensions provide a meaningful description of physical landscapes across scales and locations will be contingent on the overarching goals in any attempt to integrate ecosystem patterns more broadly.

Despite its promise, calculating fractal dimensions to measure landscape complexity has its challenges [*Halley et al.*, 2004]. These start with identifying an appropriate measure of fractal dimension but also include choosing the range of scales over which to calculate fractal dimensions, i.e. the smallest and largest scales of observation (in this study, 5 m segments and 685 – 1000 m river lengths, respectively). We identified the largest scale for each stream individually, recognising that these would then vary across streams, and used the associated fractal dimension for each for comparative purposes. Alternative choices included applying a single set of delta values (δ) for comparison across all streams, using the scale at which the maximum (or minimum) entropy value was calculated, among others. These different choices have a material effect on the resultant fractal dimensions and the ranking of streams and, therefore, are likely to affect the outcome of comparative studies. Very little published literature assists with these choices, despite their impact on the final fractal dimensions calculated. Thus, fractal dimensions should be applied thoughtfully, and additional guidance is needed to ensure that ecologists and geomorphologists apply the techniques in a mathematically robust manner.

4.5. Conclusions:

Here, the entropy fractal dimension was a meaningful measure of the complexity of ER distributions, whereas the box-counting method was less useful for comparisons among upland streams where most segments had at least one ER. The entropy fractal dimension was principally driven by the development of well-defined bed topography, for example in the form of pool-riffle sequences, as this affected longitudinal patterns of ER distribution and, to some degree, by rock size as this affected the propensity for ER to be abundant irrespective of bedform topography. Due to this ability to reflect the physical characteristics of the environment, the entropy fractal dimension shows great potential to measure the complexity of river systems in a way that is relevant to ecological processes, provided it is calculated consistently across the systems of interest.

5. Acknowledgments:

Thank you, Vicky Mak and Korbinian Strimmer, for expert advice on calculating fractal dimensions. For advice on earlier versions of the manuscript, we thank Galen Holt. For assistance collecting field data, we thank Alena Glaister, Galen Holt, Richard Mason and Harry Sanders. Thank you also to the various landowners for allowing access to Scottish field sites and to Peter Grant for facilitating access to Snobs Ck. Australian field work was carried out in conjunction with a Research Permit (No. 10007855) under the National Parks Act (Australia), from the Department of Environment, Land, Water and Planning (Victoria).

6. Funding

This research was supported by data that were originally funded by a grant from the Natural Environment Research Council, UK (NE/E004946/1) and a Discovery grant from the Australian Research Council (DP 160102262).

7. Data statement

To foster transparency, our data is available on Deakin University’s research repository.

8. References

Aubeneau, A. F., R. L. Martin, D. Bolster, R. Schumer, D. Jerolmack, and A. Packman (2015), Fractal patterns in riverbed morphology produce fractal scaling of water storage times, *Geophysical Research Letters*, *42*(13), 5309-5315.

Barnes, J. B., I. P. Vaughan, and S. J. Ormerod (2013), Reappraising the effects of habitat structure on river macroinvertebrates, *Freshwater Biology*, *58*(10), 2154-2167.

Basharin, G. P. (1959), On a statistical estimate for the entropy of a sequence of independent random variables, *Theory of Probability & Its Applications*, *4*(3), 333-336.

Bell, S. S., E. D. McCoy, and H. R. Mushinsky (2012), *Habitat structure: the physical arrangement of objects in space*, Springer Science & Business Media.

Blott, S. J., and K. Pye (2008), Particle shape: a review and new methods of characterization and classification, *Sedimentology*, *55*(1), 31-63.

Bouckaert, F. W., and J. Davis (1998), Microflow regimes and the distribution of macroinvertebrates around stream boulders, *Freshwater Biology*, *40*(1), 77-86.

Buffington, J., and D. Montgomery (2013), Geomorphic classification of rivers, in *Treatise on Geomorphology; Fluvial Geomorphology*, edited by J. Shroder and E. Wohl, pp. 730-767, Academic Press, San Diego, CA.

Butler, J. B., S. N. Lane, and J. H. Chandler (2001), Characterization of the structure of river-bed gravels using two-dimensional fractal analysis, *Mathematical Geology*, *33*(3), 301-330.

Cooper, J. R., J. Aberle, K. Koll, and S. J. Tait (2013), Influence of relative submergence on spatial variance and form-induced stress of gravel-bed flows, *Water Resources Research*, *49*(9), 5765-5777.

Cuthbert, R. N., T. Dalu, R. J. Wasserman, A. Callaghan, O. L. Weyl, and J. T. Dick (2019), Using functional responses to quantify notonectid predatory impacts across increasingly complex environments, *Acta Oecologica*, *95*, 116-119.

Davies, A., A. McAdam, and I. Cameron (1986), Geology of the Dunbar District. Memoir for Sheet 33E and Part of Sheet 41 (Scotland).

Denny, C. K., and S. E. Nielsen (2017), Spatial heterogeneity of the forest canopy scales with the heterogeneity of an understory shrub based on fractal analysis, *Forests*, *8*(5), 146-163.

Downes, B. J., T. J. Entwisle, and P. Reich (2003), Effects of flow regulation on disturbance frequencies and in-channel bryophytes and macroalgae in some upland streams, *River Research Applications*, *19*(1), 27-42.

Downes, B. J., P. S. Lake, E. Schreiber, and A. Glaister (1998), Habitat structure and regulation of local species diversity in a stony, upland stream, *Ecological Monographs*, *68*(2), 237-257.

Falconer, K. (1993), *Fractal geometry: mathematical foundations and applications*, John Wiley & Sons.

Ferreiro, N., C. Feijoó, A. Giorgi, and L. Leggieri (2011), Effects of macrophyte heterogeneity and food availability on structural parameters of the macroinvertebrate community in a Pampean stream, *Hydrobiologia*, *664*(1), 199-211.

Gordon, N. D., T. A. McMahon, B. L. Finlayson, C. J. Gippel, and R. J. Nathan (2004), *Stream Hydrology: an Introduction for Ecologists*, 2nd ed., John Wiley and Sons, West Sussex.

Halley, J., S. Hartley, A. Kallimanis, W. Kunin, J. Lennon, and S. Sgardelis (2004), Uses and abuses of fractal methodology in ecology, *Ecology Letters*, *7*(3), 254-271.

Hayes, J., and I. Jowett (1994), Microhabitat models of large drift-feeding brown trout in three New Zealand rivers, *North American Journal of Fisheries Management*, *14*(4), 710-725.

Hoover, T. M., J. S. Richardson, and N. Yonemitsu (2006), Flow-substrate interactions create and mediate leaf litter resource patches in streams, *Freshwater Biology*, *51*(3), 435-447.

Huffaker, C. (1958), Experimental studies on predation: dispersion factors and predator-prey oscillations, *Hilgardia*, *27*(14), 343-383.

Jeffries, M. (1993), Invertebrate colonization of artificial pondweeds of differing fractal dimension, *Oikos*, *67*, 142-148.

Krishnamoorthy, K., and M. Lee (2014), Improved tests for the equality of normal coefficients of variation, *Computational Statistics*, *29*(1-2), 215-232.

Lacey, R. J., and A. G. Roy (2008), The spatial characterization of turbulence around large roughness elements in a gravel-bed river, *Geomorphology*, *102*(3-4), 542-553.

Lancaster, J. (2000), Geometric scaling of microhabitat patches and their efficacy as refugia during disturbance, *Journal of Animal Ecology*, *69*(3), 442-457.

Lancaster, J., B. J. Downes, and P. Reich (2003), Linking landscape patterns of resource distribution with models of aggregation in ovipositing stream insects, *Journal of Animal Ecology*, *72*(6), 969-978.

Lancaster, J., B. J. Downes, and A. Arnold (2010), Environmental constraints on oviposition limit egg supply of a stream insect at multiple scales, *Oecologia*, *163*(2), 373-384.

Lancaster, J., B. J. Downes, R. E. Lester, and S. P. Rice (2020), Avoidance and aggregation create consistent egg distribution patterns of congeneric caddisflies across spatially variable oviposition landscapes, *Oecologia*, *192*(2), 375-389.

Lee, A., A. F. Aubeneau, and M. B. Cardenas (2020), The sensitivity of hyporheic exchange to fractal properties of riverbeds, *Water Resources Research*, *56*(5), e2019WR026560.

Lester, R. E., W. Wright, and M. Jones-Lennon (2007), Does adding wood to agricultural streams enhance biodiversity? An experimental approach, *Marine and Freshwater Research*, *58*(8), 687-698.

Mandelbrot, B. (1967), How long is the coast of Britain? Statistical self-similarity and fractional dimension, *Science*, *156*(3775), 636-638.

Mantilla, R., B. M. Troutman, and V. K. Gupta (2010), Testing statistical self-similarity in the topology of river networks, *Journal of Geophysical Research: Earth Surface*, *115*(F3).

Marsden, M. A. H. (1973), Palaeozoic evolution of east-central Victoria: Regional Guide to Victorian Geology, edited by M. McAndrew and M. A. H. Marsden, pp. 175-201.

Marwick, B., and K. Krishnamoorthy (2018), cvequality: Tests for the Equality of Coefficients of Variation from Multiple Groups, *R software package version 0.1*, *3*.

Meager, J. J., and T. A. Schlacher (2013), New metric of microhabitat complexity predicts species richness on a rocky shore, *Marine Ecology*, *34*(4), 484-491.

Miller, G. (1955), Note on the bias of information estimates, in *Information Theory in Psychology: Problems and Methods*, edited by H. Quastler, pp. 95–100, The Free Press, Glencoe.

Monsalve, A., E. M. Yager, and M. W. Schmeeckle (2017), Effects of bed forms and large protruding grains on near-bed flow hydraulics in low relative submergence conditions, *Journal of Geophysical Research: Earth Surface*, *122*(10), 1845-1866.

Montgomery, D. R., and J. M. Buffington (1997), Channel-reach morphology in mountain drainage basins, *Geological Society of America Bulletin*, *109*(5), 596-611.

Nikora, V. I. (1991), Fractal structures of river plan forms, *Water Resources Research*, *27*(6), 1327-1333.

Ossola, A., A. K. Hahs, M. A. Nash, and S. J. Livesley (2016), Habitat complexity enhances comminution and decomposition processes in urban ecosystems, *Ecosystems*, *19*(5), 927-941.

Papanicolaou, A., A. G. Tsakiris, M. A. Wyssmann, and C. M. Kramer (2018), Boulder array effects on bedload pulses and depositional patches, *Journal of Geophysical Research: Earth Surface*, *123*(11), 2925-2953.

Petersen, I., and A. G. Hildrew (2003), Emergence of *Leuctra nigra* (Plecoptera) from a southern English stream, *Archiv für Hydrobiologie*, *158*(2), 185-195.

R Core Team (2019), R: A language and environment for statistical computing

Reich, P. (2004), Patterns of composition and abundance in macroinvertebrate egg masses from temperate Australian streams, *Marine and Freshwater Research*, *55*(1), 39-56.

Rice, S. P. (2017), Tributary connectivity, confluence aggradation and network biodiversity, *Geomorphology*, *277*, 6-16.

Rice, S. P., and M. Church (1996), Bed material texture in low order streams on the Queen Charlotte Islands, British Columbia, *Earth Surface Processes Landforms*, *21*(1), 1-18.

Rice, S. P., and M. Church (1998), Grain size along two gravel-bed rivers: statistical variation, spatial pattern and sedimentary links, *Earth Surface Processes Landforms: The Journal of the British Geomorphological Group*, *23*(4), 345-363.

Rinaldo, A., I. Rodriguez-Iturbe, R. Rigon, R. L. Bras, E. Ijjasz-Vasquez, and A. Marani (1992), Minimum energy and fractal structures of drainage networks, *28*(9), 2183-2195.

Ritchie, M. E. (2009), *Scale, heterogeneity, and the structure and diversity of ecological communities*, Princeton University Press.

Rodríguez-Iturbe, I., and A. Rinaldo (2001), *Fractal river basins: chance and self-organization*, Cambridge University Press.

Sapozhnikov, V., and E. Foufoula-Georgiou (1996), Self-affinity in braided rivers, *Water Resources Research*, *32*(5), 1429-1439.

Seuront, L. (2009), *Fractals and multifractals in ecology and aquatic science*, CRC Press.

Seuront, L., and Y. Lagadeuc (1997), Characterisation of space-time variability in stratified and mixed coastal waters (Baie des Chaleurs, Québec, Canada): application of fractal theory, *Marine Ecology Progress Series*, *159*, 81-95.

Shen, X., L. Zou, G. Zhang, N. Su, W. Wu, and S. Yang (2011), Fractal characteristics of the main channel of Yellow River and its relation to regional tectonic evolution, *Geomorphology*, *127*(1-2), 64-70.

Singh, A., S. Lanzoni, P. R. Wilcock, and E. Foufoula-Georgiou (2011), Multiscale statistical characterization of migrating bed forms in gravel and sand bed rivers, *Water Resources Research*, *47*(12).

Singh, A., K. Fienberg, D. J. Jerolmack, J. Marr, and E. Foufoula-Georgiou (2009), Experimental evidence for statistical scaling and intermittency in sediment transport rates, *Journal of Geophysical Research: Earth Surface*, *114*(F1).

Stewart, M. T., S. M. Cameron, V. I. Nikora, A. Zampiron, and I. Marusic (2019), Hydraulic resistance in open-channel flows over self-affine rough beds, *Journal of Hydraulic Research*, *57*(2), 183-196.

Strobl, C. (2005), Variable selection in classification trees based on imprecise probabilities, *ISIPTA*, *5*, 340-348.

Tarboton, D. G. (1989), The analysis of river basins and channel networks using digital terrain data, Massachusetts Institute of Technology.

Wang, B., F. Tian, and H. Hu (2009), Relationship between fractal dimension of river networks and their climates, *Journal of Tsinghua University Science Technology*, *49*(12), 1948-1953.

Warfe, D., L. Barmuta, and S. Wotherspoon (2008), Quantifying habitat structure: surface convolution and living space for species in complex environments, *Oikos*, *117*(12), 1764-1773.

Wiens, J. A. (1989), Spatial scaling in ecology, *Functional Ecology*, *3*(4), 385-397.

Wolman, M. G. (1954), A method of sampling coarse river-bed material, *EOS, Transactions American Geophysical Union*, *35*(6), 951-956.

Wu, F.-C., C.-K. Wang, and G.-H. Huang (2018), Delineation of gravel-bed clusters via factorial kriging, *Geomorphology*, *308*, 161-174.

Yang, H., and C. Shi (2017), The fractal characteristics of drainage networks and erosion evolution stages of ten kongduis in the upper reaches of the Yellow River, *Journal of Resources and Ecology*, *8*(2), 165-173.

Zhang, S., Y. Guo, and Z. Wang (2015), Correlation between flood frequency and geomorphologic complexity of rivers network–a case study of Hangzhou China, *Journal of hydrology*, *527*, 113-118.

Zhong, L., F. Zeng, and G. Xu (2012), Comparison of fractal dimension calculation methods for channel bed profiles, *Procedia Engineering*, *28*, 252-257.

AGU PUBLICATIONS

Water Resources Research

Supporting Information for

Using fractals to describe ecologically-relevant patterns in distributions of large rocks in streams

G. K. Dwyer[1], C. R. Cummings[1], S. P. Rice[2], J. Lancaster[3], B. J. Downes[3], L. Slater[4], and R. E Lester[1]

1Centre for Regional and Rural Futures, Deakin University, Locked Bag 20000, Geelong, Vic. 3220, Australia.

2 Department of Geography, Loughborough University, Loughborough, LE11 3TU, U.K.

3 School of Geography, The University of Melbourne, Victoria, Australia

4School of Geography and the Environment, University of Oxford, South Parks Road, Oxford OX1 3QY, UK

Contents of this file

Additional Supporting Information (Files uploaded separately)

Captions for Script S1 - R scripts for calculating fractal dimensions
Captions for Script S2 - R scripts for simulating synthetic stream stretches

Text S1.

Calculating fractal dimensions

The calculation of the fractal dimensions involved the following five steps:

1) Calculate N_X for all possible values of δ;
2) Log-transform linear regression of δ and N_X;
3) R^2 – SSR Procedure;
4) Zero-slope Procedure;
5) Compensated-Slope Procedure

Step 1: Calculation of N_X for all possible values of δ

All possible values of δ were identified. This is simply a sequence of values from the smallest scale of observation (here, 5 m segments) to the largest scale of observation (here, the study sites ranged from 685 – 1000 m) increasing in increments of the smallest scale. For example, the box sizes used for Dye are as follows:

δ: 5, 10, 15, …, 990, 995, 1000.

For each value of δ, the dataset was divided into boxes of size δ to calculate N_X. As the data collected for each stream is 1-dimensional, the stream section is divided in only that one direction, along the length of the site. For the box-counting method, N_B is calculated as the number of occupied boxes. Irregularities in the ER distributions of a size smaller than δ are disregarded in box sizes greater than δ (Seuront, 2009). For example, sections without rocks that were 10 m in length (2 segments) would be ignored at values of delta greater than 15 m (3 segments). As a result, the values of N_B using the box-counting method on the Dye dataset, which does not contain any segments without ER, are as follows:

Dye values of N_B: 200, 100, 67, …, 2, 2, 1.

For the entropy method, N_E is calculated using the proportions of the total ER, following weighting and correction for bias in the estimate of entropy as per Miller (1955) and Basharin (1959). The weighted estimate (*H*; theoretical Shannon entropy) was calculated as:

$$H = -\sum p \times \log_e p$$

where *p* is the proportion of total ER in each box. The correction for bias in the estimate of entropy as per Miller (1955) and Basharin (1959) was achieved according to the following equation:

$$\log N_E = \propto H + \frac{(s-1)}{2N} \times \log_2 e$$

where *s* is sample size (number of boxes) and *N* is the total number of ER. The constant $\log_2(e)$ has a value of 1.442695. ∝ indicates that we neglect terms of the order of $O\left(\frac{1}{N^2}\right)$; this correction provides a decent approximation of the true entropy value, but only for sufficiently large sample sizes (Strobl, 2005). Further, the correction is negligible for N to infinity (Strobl, 2005). For example, the values of N_E using the entropy method on the Dye dataset are as follows:

Log N_E: 4.97, 4.31, 3.92, …, 0.00, 0.00, 0.00.

The list of δ and associated N_X was condensed to remove duplicate and inconsequential values of N_X. Using the Dye dataset for instance, δ values of 100, 105, and 110 all result in N_B of 10 and δ values between 500 and 995 all result in an N_B of 2. Further using the entropy method, δ values were removed where the resulting value for log N_E equalled 0, as this indicates that the entire data set fit into fewer than two boxes. The final condensed list (of δ and N_X) is used in the remaining four steps to provide an estimate of fractal dimensions (D_X) including Seuront's (2009) three-step procedure to confirm the presence of fractal-like properties in the ER distributions.

Step 2: Log-transformed linear regression
Simple linear regression of log(δ) and log(N_X) provides a first estimate of the fractal dimension. The slope of the linear regression estimated over the values of δ provides an estimate of the scaling exponent (D_X) (Fig. S1A)

Step 3: R^2 – SSR Procedure
The R^2 – SSR Procedure estimates D_X by using the values of δ which simultaneously maximised the coefficient of determination (R^2) and minimized the total sum of the squared residuals (SSR) (Seuront & Lagadeuc, 1997) (Fig. S1B). This was achieved by looping over the list of δ and N_X with a 'regression window'. Similar to the 'boxes' used to loop over the ER counts to calculate N_X, the regression window looped over the list of δ and N_X to allow calculation of the R^2 and SSR for each window. The range of window sizes used here ranged from a minimum of six data points to a maximum that contained the entire list. The R^2 – SSR criterion was only satisfied if the largest R^2 value and smallest SSR value were produced from the same regression window (Seuront & Lagadeuc, 1997). An estimate of D_x was then calculated from the slope of the points contained in the regression window that satisfied the R^2 – SSR criterion. This process ensures that artefacts of linearity in the log-log plot (e.g. due to power-law relationships) are avoided.

Step 4: Zero-slope Procedure
The Zero-slope Procedure provides an estimate of D_X from the intersection of a fitted line of zero-slope with the axis describing the derivative of log(N_X) with respect to log(δ) (Fig. 1C). Again a sliding regression window is used to determine whether the slope of the derivative of log(N_X) with respect to log(δ) for any regression window is significantly different from zero. To satisfy the criterion of the Zero-Slope Procedure, the slope of all windows must not be significantly different from zero. An estimate of D_X is calculated from the intercept, using the largest window where the slope was not significantly different to zero. This procedure has a disadvantage in that enhanced noise is generated by taking the first derivative of any linear trend which causes problems for standard statistical procedures; however this is overcome in the following compensated-slope procedure.

Step 5: Compensated-Slope Procedure
The Compensated-Slope Procedure estimates D_X from a range of compensated exponents. The compensated exponent which best estimates D_X is determined by the plot of $\log\,[\,\delta^{C} \times \delta^{-D_X}]$ versus $\log$ (δ), where the slope is closest to zero (Fig. 1D). The estimate of D_X used for this procedure is produced from the linear regression of log(δ) and log(N_X) in step 2. We used 101 values of C that ranged from 0 to D_X+1, to allow an excess of values extending into the next dimension. The value of C whereby the slope was closest to zero was used as the D_X estimate in the in the current paper, as plateau behaviour in this relationship is a manifestation of scaling and therefore should not be the result of random non-fractal structure (i.e. an artefact of the data). The Compensated-Slope criterion was only satisfied if the slope was not significantly different from zero.

As stated by Seuront (2009), fractal-like behaviour is only confirmed if the criteria of two of the three test procedures described above are satisfied. R scripts for the calculation of the fractal dimensions are found in Supporting Information Script S1.

References

Basharin, G. P. (1959). On a statistical estimate for the entropy of a sequence of independent random variables. *Theory of Probability & Its Applications, 4*(3), 333-336.

Miller, G. (1955). *Note on the bias of information estimates.* . Glencoe, IL: Free Press.

Seuront, L. (2009). *Fractals and multifractals in ecology and aquatic science*: CRC Press.

Seuront, L., & Lagadeuc, Y. (1997). Characterisation of space-time variability in stratified and mixed coastal waters (Baie des Chaleurs, Québec, Canada): application of fractal theory. *Marine Ecology Progress Series, 159*, 81-95.

Strobl, C. (2005). *Variable Selection in Classification Trees Based on Imprecise Probabilities.* Paper presented at the ISIPTA.

Text S2.

Simulating emergent rocks in streams

Synthetic stream stretches were simulated using base R (R Foundation for Statistical Computing, Vienna, Austria) using the characteristics observed in the six study streams. These characteristics included: 1) site length, 2) feature (riffle and pool) lengths and 3) the number of ER in the 5-m segments.

To produce the synthetic stream stretches: First, a sequence of feature lengths was produced by alternately selecting riffle and pools lengths (X_{rL} and X_{pL}) from log-normal distributions, calculated based on the study stream data, until the cumulative length exceeded stream length (e.g. a sequence may include 3_{pL}, 7_{rL}, 10_{pL}, 21_{rL}, 4_{pL}, 22_{rL}, 3_{pL}, 7_{rL}, 6_{pL}, 7_{rL}..., indicating that the first feature was a pool of length 3m and the next feature was a riffle of length 7 m, and so on). The parameters of these distributions were μ = 1.372 and 2.049, and σ = 0.571 and 0.829 for pools and riffles, respectively. Next, the sequence of riffle and pool lengths was translated into a binary sequence, with each digit (r or p) representing a single 5-m segment (e.g. for the above example, the binary sequence would begin with p, p, p, r, r, r, r, r, r, r, and so on). Finally, digits (r and p) of the binary sequence were replaced with values selected from negative binomial distributions based on the ER numbers in either riffles or pools of the study streams. These values represent the number of ER in each 5-m segment (e.g. 36_{pER}, 11_{pER}, 2_{pER}, 71_{rER}, 48_{rER}, 10_{rER}, 99_{rER}, 74_{rER}, 16_{rER}, 30_{rER}...., indicates that the first 5-m segment in the example sequence above was a pool with 36 ER, the next segment was also part of the same pool but with 11 ER, given that the first pool extended for three segments in the stream length sequence, and so on). Two riffle/pool sets of ER distributions were used for the simulations, one fitted from the low-zero streams (low-zero streams; including Kelphope and Faseny) and one from the high-zero streams (high-zero streams; including Dye, Steavenson, Snobs, and Little) (Fig. S2). The parameters of the ER distributions for the low-zero streams were: size = 1.28 and 1.64, and μ = 43.2 and 60.1 for riffles and pools, and for the high-zero streams: size = 0.266 and 0.638 and μ = 5.46 and 14.8 for riffles and pools.

To determine the effect of each stream characteristic on fractal dimension, each characteristic was manipulated individually, leading to a total of 640 synthetic streams (see Fig. S3 for an example). A default of 1000 m was used for the length of synthetic stream stretches. However, to test for any influence of site length on fractal dimensions (D_x) site length 'variants' of 685, 765, 845, 920, and 1000 m were used, which spans the observed range. Variants of feature lengths were produced using multipliers (1, 2, 4, and 8) on riffle and pool lengths separately. Variants of ER density were produced using multipliers (1, 2, 4, and 8) on riffle ER counts separately, and pool and riffle ER counts simultaneously. Pool length and riffle ER density were also manipulated simultaneously (using multipliers 1, 2, 4, and 8 on both; Fig. S3). Further simulations were produce by adding systematic features with segments containing zero ER (including features of length 1 [every second segment has zero ER], 2 [two segments with ER, two segments with zero ER], 5, 10, 15, 20, 30, 40, 50, 60, 70, 80, 90 and 100), Each set of simulations included 10-20 replicates of each variant; i.e. for the set of simulations for which site length was manipulated, 5 variants (685, 765, 845, 920, and 1000 m) were produced, with 10 replicates of each, equating to a total of 50 synthetic stream stretches.

R scripts for simulating synthetic stream stretches are found in Supporting Information (Script S2).

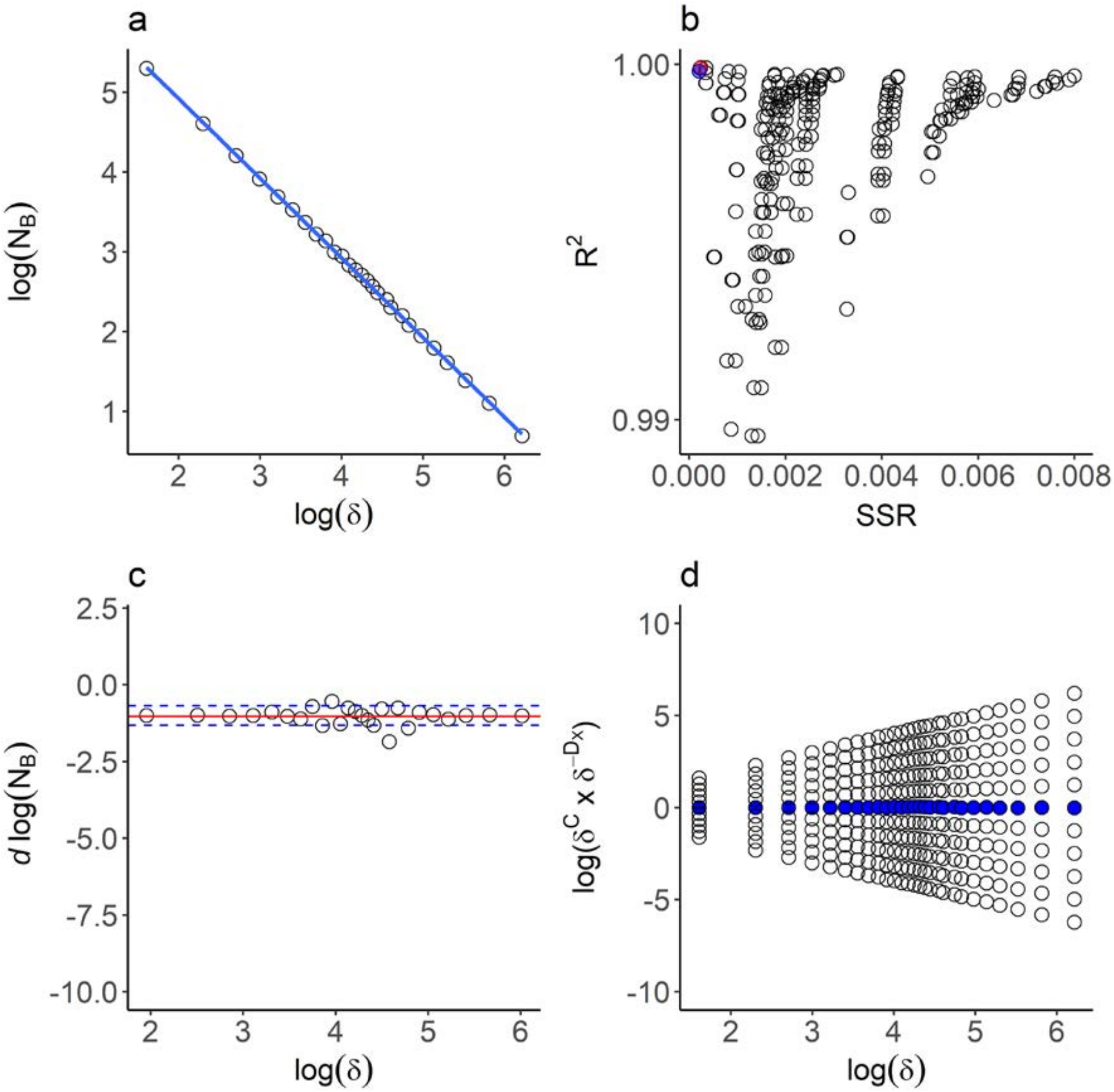

Figure S1. Four methods of calculating fractal dimensions using the box-counting method with the Dye dataset for example. **(a)** Log-transformed linear regression of δ and N_B. **(b)** The R^2 – SSR Procedure. Each point shows R^2 and the SSR for each regression window. Here, the R^2 – SSR criterion were not met as the regression window with the highest R^2 (red shaded point) and the regression window with the lowest SSR (blue shaded point) were not one and the same. **(c)** The Zero-slope Procedure. Here the derivative of log(N_B) is plotted against log(δ). The red solid line gives the best estimate of D_x and the blue dashed line provide confidence intervals based on the largest and smallest plausible values of D_x for these data **(d)** The Compensated-Slope Procedure. Here $\log\left[\boldsymbol{\delta^{C}} \times \boldsymbol{\delta^{-D_X}}\right]$ is plotted against log(δ). The compensated exponent which best estimates D_X is where the slope is closest to zero (blue filled points). Methods **b – d** are required for Seuront's (2009) three-step procedure to confirm the presence of fractal-like properties.

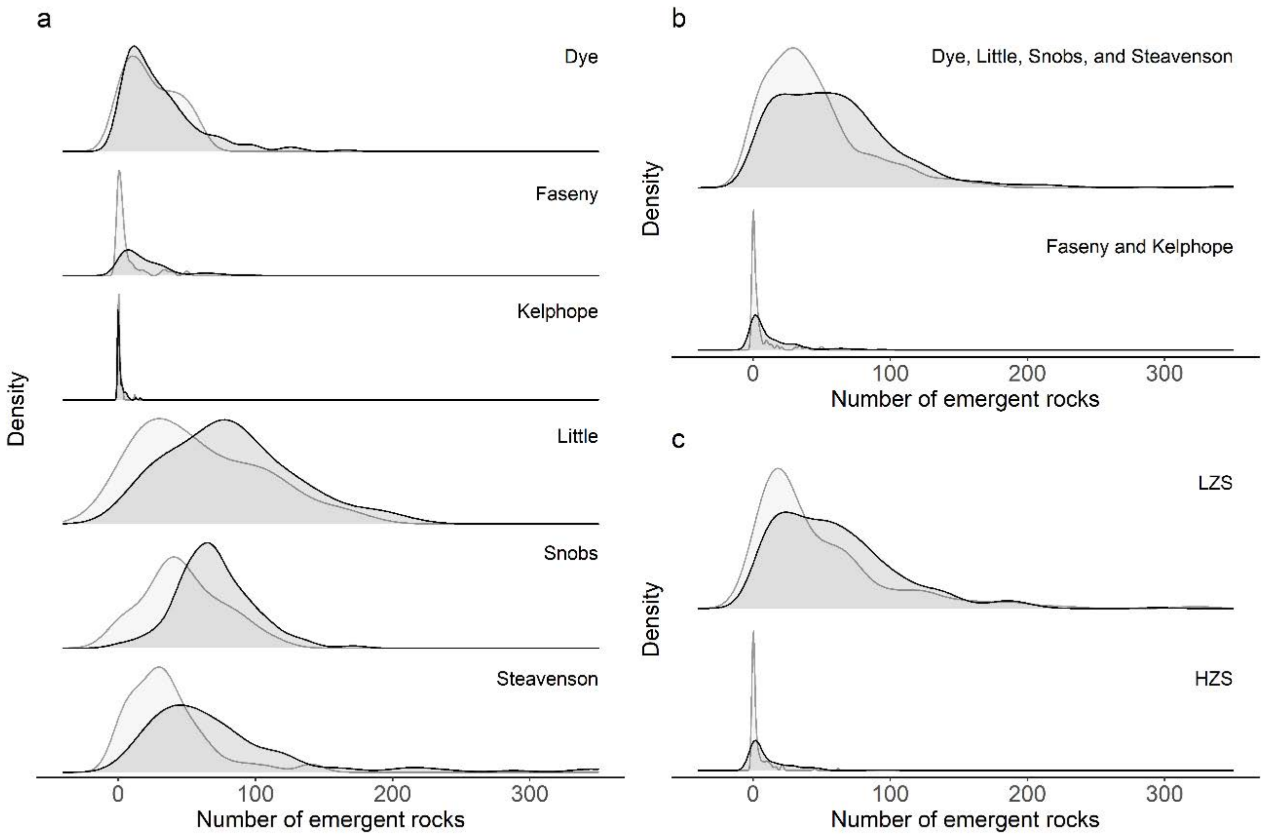

Figure S2. Frequency distributions of ER in riffles (dark grey) and pools (light grey) of **(a)** each stream individually, **(b)** grouped low-zero streams (low-zero streams) including Dye, Little, Snobs, and Steavenson and grouped high-zero streams, including Faseny and Kelphope, and **(c)** simulated data using negative binomial distributions fitted to the low-zero streams and high-zero streams data.

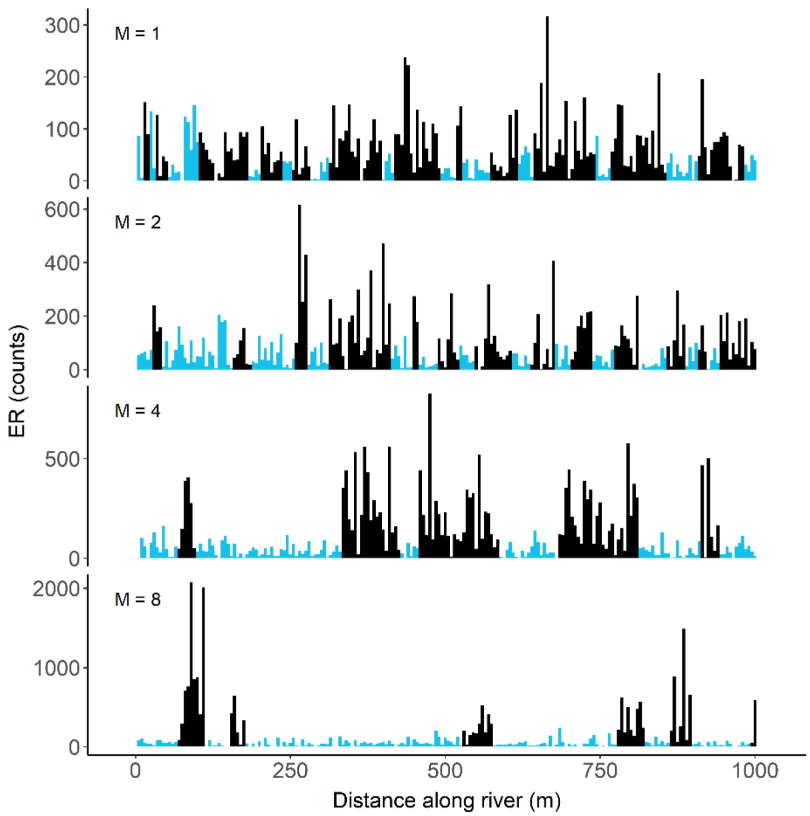

Figure S3. Example of four synthetic stream stretches where pool lengths and riffle ER density have been manipulated simultaneously using multipliers (M) of 1, 2, 4, or 8. Segments of pools (blue) and riffles (black) are 5 m in length and span a 1000 m stream stretch.

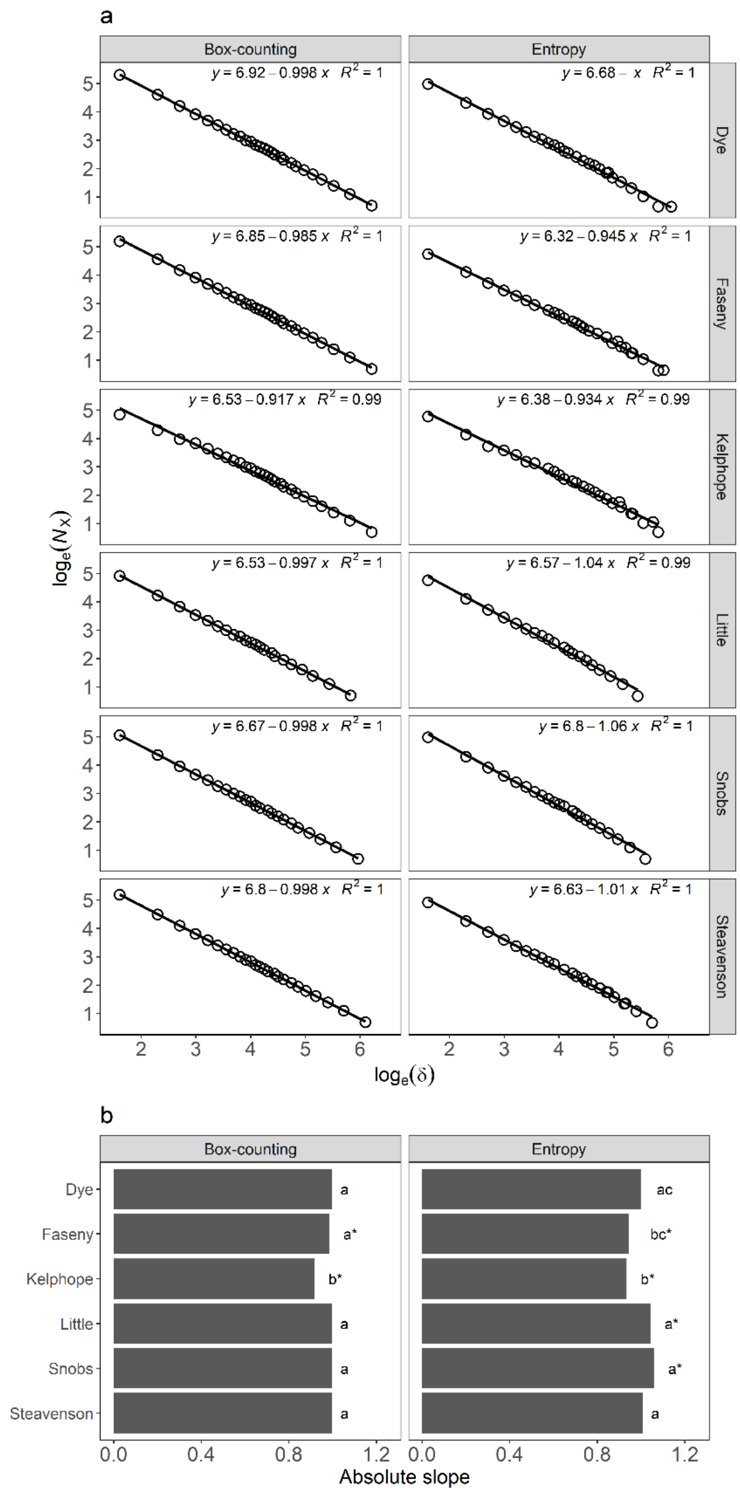

Figure S4. (a) Log-log plots and **(b)** a comparison of the corresponding absolute slopes for the box counting dimension (left columns) and the entropy dimension (right columns) for ER counts in the six study streams. Significant differences among streams are signified with lower-case letters (e.g. for the box-counting method Kelphope was significantly different to all other streams) and were determined using post hoc analysis tests using the 'lstrends' r package. Asterisks signify a significant difference from a slope of one, tests of which were executed using two-tailed linear regression analyses with an offset term fixed at -1. Equations are presented in log-transformed units.

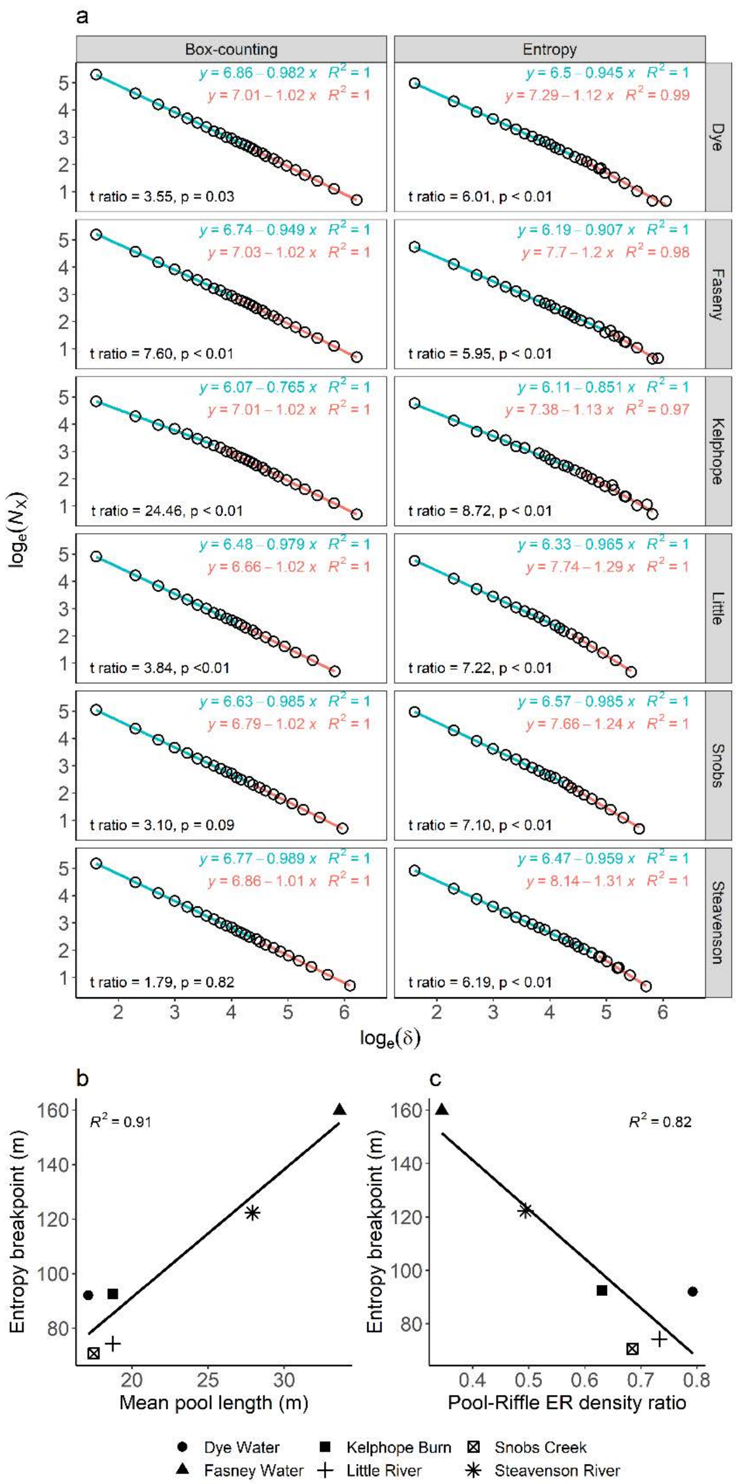

Figure S5. Exploring multiple scaling. **(a)** Log-log plots for the box counting dimension (left columns) and the entropy dimension (right columns) for ER counts in the six study streams. Data were divided at breakpoints that were identified using the r package 'segmented' that identifies where the linear relation changes using bootstrap restarting. Significant differences between the small- (blue lines and equations) and large-scale (red lines and equations) slopes for each stream were determined using post hoc analysis tests using the 'lstrends' r package. Equations are presented in log-transformed units. Breakpoints were significantly related to pool-riffle structure as seen with the relation between (b) pool lengths and (c) pool-riffle ER density ratio. Breakpoints were not related to channel width or stream length.

Table S1. Rationale for directional hypotheses.

Characteristic (Expected direction)	Propensity for rocks to emerge and thence the number of ER	Bedform development and thence the spatial organisation of ER
Stream morphology		
Median depth (Negative)	Rocks are less likely to be emergent in deeper topography (fewer ER)	Depth increases downstream and is associated with better bedform development
Stream slope (Positive)	Greater slopes are associated with larger bed materials (more ER)	Slope decreases downstream and is associated with better bedform development
Mean proportional pool length (Negative)	Longer pool length implies greater occurrence of deeper topography (fewer ER)	Longer pool lengths imply stronger organisation of bed topography
Mean proportional riffle length (Positive)	Longer riffle-like length implies greater occurrence of shallow topography (more ER)	NA
Number of pool-riffle transitions (Negative)	NA	The number of pool-riffle transitions implies greater bed form development and structure
Bed sediment		
Axis B (Positive)	For a given water depth, larger bed materials are more likely to be emergent (more ER)	Larger bed materials are more common in steeper channels. Slope decreases downstream and is associated with reduced bedform development
Axis C (Positive)	Larger c-axis increases elevation above the average bed surface because most grains rest on their a-b plane (more ER)	Larger bed materials are more common in steeper channels. Slope decreases downstream and is associated with reduced bedform development
Equancy ratio (C/A) (Positive)	Greater equancy increases elevation above the average bed surface (more ER)	NA
Flatness ratio (C/B) (Negative)	Greater flatness decreases elevation above the average bed surface (fewer ER)	NA
ER density measures		
Mean ER density (Positive)	ER density is directly related to the number of ER	NA
Pool-riffle ER density ratio (Negative)	NA	Pool-riffle ER density ratio is directly related to spatial organisation of ER
Segments without ER		
Number of segments without ER (Negative)	Number of segments without ER is directly related to the number of segments with ER	Coarse measure of the number of pools, implies strong organisation of bed topography
Maximum length without ER (Negative)	Maximum length without ER is directly related to the number of segments with ER	Coarse measure of longest pool, implies strong organisation of bed topography

Table S2. Proportions of channel morphologies in the six study streams.

	Scotland			Australia		
	Dye	**Faseny**	**Kelphope**	**Little**	**Snobs**	**Steavenson**
Pools	0.14	0.40	0.27	0.34	0.19	0.38
Riffle-like	0.86	0.60	0.73	0.66	0.81	0.62
True riffle	0.00	0.04	0.40	0.41	0.07	0.50
Plane Bed	0.86	0.56	0.33	0.25	0.65	0.12
Step Pool	0.00	0.00	0.00	0.00	0.09	0.00

Note. Simplified morphology into pools and 'riffle-like', provide a high-level distinction between deeper pools and those sections where the flow is relatively shallow and bed materials are more likely to be exposed. The 'riffle-like' category is the sum of true riffles, plane beds, step-pools. See Methods, section 2.3.

Table S3. Geographical and physical features of the study streams along the survey lengths. Where relevant, values are reported as mean ± SD. SR indicates submerged rocks.

	Scotland			Australia		
	Kelphope	**Faseny**	**Dye**	**Snobs**	**Little**	**Steavenson**
Latitude	N 55.78639	N 55.85111	N 55.81528	S 37.27382	S 37.34908	S 37.48389
Longitude	W 2.78389	W 2.59194	W 2.57222	E 145.87713	E 145.75202	E 145.75242
Altitude (m)	230	300	270	283	308	379
Survey length (m)	1000	1000	1000	785	685	885
Stream morphology						
Mean channel width (m)	2.5 ± 0.5	5.8 ± 1.7	6.6 ± 1.3	5.8 ± 1.4	6.1 ± 1.7	9.5 ± 2.6
Median depth (m)	0.13	0.22	0.23	0.36	0.30	0.37
Slope (%)	0.94	1.04	1.09	3.08	1.47	1.01
Mean proportional riffle lengths	0.10 ± 0.06	0.05 ± 0.03	0.11 ± 0.13	0.09 ± 0.09	0.06 ± 0.03	0.05 ± 0.05
Mean proportional pool lengths	0.04 ± 0.02	0.04 ± 0.02	0.02 ± 0.01	0.02 ± 0.01	0.03 ± 0.02	0.03 ± 0.02
Pool-riffle transitions	25	2	14	19	26	24
Bed sediment						
ER axis A (mm)	191.5 ± 52.2	375.3 ± 153.9	371.6 ± 117.2	290.7 ± 152.7	256.4 ± 110.8	202.9 ± 106.3
ER axis B (mm)	126.3 ± 33.6	241.2 ± 89.9	253.9 ± 74.7	203 ± 102.9	185.7 ± 74.4	147.8 ± 72.2
ER axis C (mm)	76.9 ± 31.9	134.1 ± 73.3	122.1 ± 54.3	147.2 ± 83.5	121.2 ± 59.1	95.2 ± 57.1
ER elongation ratio	0.68 ± 0.15	0.67 ± 0.17	0.71 ± 0.17	0.71 ± 0.13	0.74 ± 0.13	0.75 ± 0.13
ER flatness ratio	0.61 ± 0.20	0.57 ± 0.24	0.50 ± 0.22	0.73 ± 0.16	0.66 ± 0.19	0.65 ± 0.19
ER equancy ratio	0.41 ± 0.14	0.37 ± 0.16	0.34 ± 0.14	0.52 ± 0.14	0.48 ± 0.14	0.48 ± 0.15
SR axis A (mm)	136.1 ± 43.8	202.2 ± 97.9	220.6 ± 103.8	187.1 ± 82.5	178.2 ± 79.1	160.4 ± 87.4
SR axis B (mm)	93.7 ± 31.5	134.7 ± 67.4	152.3 ± 69.6	139.6 ± 62.6	133.8 ± 59.6	115.4 ± 63.5
SR axis C (mm)	42.6 ± 19.1	58.6 ± 37.1	65 ± 32.3	94.6 ± 47.9	87.2 ± 40.3	73.7 ± 43.3
SR elongation ratio	0.70 ± 0.15	0.68 ± 0.15	0.71 ± 0.15	0.76 ± 0.12	0.76 ± 0.12	0.73 ± 0.14
SR flatness ratio	0.47 ± 0.19	0.44 ± 0.19	0.46 ± 0.19	0.68 ± 0.15	0.66 ± 0.16	0.65 ± 0.18
SR equancy ratio	0.32 ± 0.12	0.30 ± 0.13	0.31 ± 0.12	0.51 ± 0.13	0.50 ± 0.13	0.47 ± 0.14
ER density measures						
Density of ER (no. m^{-2})	0.31	0.57	1.01	2.31	2.44	1.27
Pool-riffle ER density ratio	0.63	0.34	0.79	0.68	0.73	0.49
Segments without ER						
Number of segments without ER	109	34	0	0	2	1
Maximum length without ER (m)	50	25	<5	<5	5	5

Table S4. Correlation tests among variables describing physical features of the study streams. All tests are two-tailed with DF = 4. r-values significant at $\alpha < 0.05$ are shown in bold. Sets of cells in shaded grey describe similar aspects of the stream: stream bed morphology, sediment size and shape, and ER density. Cells shaded yellow indicate significant correlations among different aspects. SR indicates submerged rocks.

	Median depth	Slope	Mean length riffles	Mean length pools	Pool-riffle transitions	ER axis B	ER axis C	ER flatness	ER equancy	SR axis B	SR axis C	SR flatness	SR equancy	ER density	ER density ratio	Segments without ER
Median depth																
Slope	0.549															
Mean proportional riffle length	-0.426	0.184														
Mean proportional pool length	-0.581	-0.593	-0.421													
Pool-riffle transitions	0.215	0.095	0.145	-0.146												
ER axis B	0.028	0.136	0.097	-0.397	-0.779											
ER axis C	0.437	0.662	-0.09	-0.505	-0.541	0.780										
ER flatness	0.621	0.718	-0.274	-0.141	0.499	-0.48	0.173									
ER equancy	0.734	0.66	-0.301	-0.252	0.603	-0.491	0.128	**0.972**								
SR axis B	0.362	0.358	0.082	-0.687	-0.487	**0.909**	**0.849**	-0.216	-0.164							
SR axis C	**0.875**	0.753	-0.221	-0.684	0.222	0.193	0.656	0.653	0.73	0.547						
SR flatness	**0.862**	0.614	-0.31	-0.451	0.602	-0.33	0.213	**0.856**	**0.948**	0.059	**0.859**					
SR equancy	**0.847**	0.632	-0.316	-0.441	0.585	-0.304	0.249	**0.863**	**0.947**	0.082	**0.874**	**0.997**				
ER density	0.753	0.687	-0.166	-0.608	0.396	0.071	0.53	0.662	0.744	0.444	**0.958**	**0.867**	**0.892**			
ER density ratio	0.018	0.297	0.712	-0.67	0.528	0.044	0.034	0.009	0.100	0.284	0.312	0.233	0.242	0.457		
Segments without ER	**-0.823**	-0.379	0.272	0.734	0.096	-0.519	-0.654	-0.155	-0.295	-0.788	**-0.813**	-0.548	-0.547	-0.694	-0.189	
Max length without ER	**-0.813**	-0.450	0.107	**0.845**	-0.009	-0.478	-0.621	-0.177	-0.324	-0.781	**-0.831**	-0.579	-0.575	-0.727	-0.347	**0.982**

Table S5. Fractal Dimension Results using the Box-Counting and Entropy Methods.

	Scotland			Australia		
	Dye	**Faseny**	**Kelphope**	**Little**	**Snobs**	**Steavenson**
Box-Counting						
Log(δ)-log(N_B) slope	**1.00**	**0.98**	**0.92**	**1.00**	**1.00**	**1.00**
R^2 – SSR	0.99	0.95	**1.01**	0.99	**0.99**	**0.99**
Zero-Slope	**1.03**	**1.02**	**0.97**	**1.03**	**1.02**	**1.02**
Compensated-Slope (D_B)	**1.00**	**0.97**	**0.90**	**1.00**	**1.00**	**1.00**
Entropy						
Log(δ)-log(N_E) slope	**1.00**	**0.94**	**0.93**	**1.04**	**1.06**	**1.01**
R^2 – SSR	**0.94**	0.91	**1.03**	0.96	**0.98**	**0.96**
Zero-Slope	**0.98**	**0.98**	**1.19**	**1.11**	**1.10**	**0.99**
Compensated-Slope (D_E)	**1.00**	**0.93**	**0.91**	**1.02**	**1.05**	**0.98**

Note. One estimate of fractal dimension can be produced from the absolute slope of log(δ)-log(N_X) linear regression, where significant linearity (here indicated with bold text) indicates the likely presence of a fractal structure. A more robust method of confirming the presence of fractal-like properties follows *Seuront's* [2009] three-step procedure, including the 1) R^2 – SSR, 2) Zero-Slope, and 3) Compensated-Slope procedures. Using this method, any stream must satisfy any two of the three criteria to be considered fractal [*Seuront*, 2009] (see Supporting Text S1). Bold text indicates that the data satisfy the criterion for the test in question. Plain text indicates that the data did not satisfy the criterion. As described in the methods above, D_X was selected using the Compensated-Slope Procedure, as indicated by the parentheses.

Table S6. One-tailed correlation tests of the study stream characteristics with the box-counting and entropy fractal dimensions. DF = 4. Bold text indicates $p < 0.05$.

	Expected direction	Box-counting		Entropy	
		r	p	r	p
Stream morphology					
Median depth	Negative	0.817	0.977	0.791	0.969
Stream slope	Positive	0.365	0.238	**0.737**	**0.047**
Mean proportional pool length	Negative	-0.709	0.057	**-0.870**	**0.012**
Mean proportional riffle length	Positive	-0.301	0.719	0.054	0.460
Number of pool-riffle transitions	Negative	-0.124	0.408	0.241	0.677
Bed sediment					
ER axis B	Positive	**0.791**	**0.030**	0.653	0.080
ER axis C	Positive	**0.804**	**0.027**	**0.950**	**0.002**
ER equancy ratio (C/A)	Positive	0.534	0.137	**0.765**	**0.038**
ER flatness ratio (C/B)	Negative	0.534	0.862	0.755	0.958
SR axis B	Positive	0.532	0.139	0.291	0.288
SR axis C	Positive	0.663	0.076	0.636	0.087
SR equancy ratio (C/A)	Positive	0.283	0.294	0.582	0.113
SR flatness ratio (C/B)	Negative	0.146	0.609	0.482	0.833
ER density measures					
ER density over entire site	Positive	0.679	0.069	**0.917**	**0.005**
Pool-riffle ER density ratio	Negative	0.157	0.617	0.541	0.866
Segments without ER					
Number of segments without ER	Negative	**-0.999**	**<0.001**	**-0.832**	**0.020**
Maximum length without ER	Negative	**-0.974**	**0.001**	**-0.895**	**0.008**

Table S7. Linear regression tests of the log(δ) versus log(N_X) for the box-counting (N_B) and entropy (N_E) methods. Linearity indicates the likely presence of fractal structure.

	Box-counting				Entropy			
River	**F-statistic**	**DF**	**p-value**	**R^2**	**F-statistic**	**DF**	**p-value**	**R^2**
Dye	84177	25	<0.01	1.00	6263	24	<0.01	1.00
Faseny	34778	25	<0.01	1.00	6208	25	<0.01	1.00
Kelphope	3498	25	<0.01	0.99	2604	24	<0.01	0.99
Little	47493	20	<0.01	1.00	2901	18	<0.01	0.99
Snobs	63688	21	<0.01	1.00	4434	20	<0.01	1.00
Steavenson	151983	23	<0.01	1.00	5399	22	<0.01	1.00

Table S8. Linear regression tests of the stream characteristics using synthetic stream stretches with the box-counting and entropy fractal dimensions. Entropy results are repeated for ease of comparison.

Independent variable	Manipulated variable(s)	ER dist.	DF	Box counting				Entropy			
				Slope	t-value	p-value	$R^{2\wedge}$	Slope	t	p	R^2
Stream morphology											
Mean proportional pool length	Pool lengths	LZS	78	-2.6×10^{-8}	0.08	0.94	<0.01	**-8.9×10^{-5}**	**3.48**	**<0.001**	**0.13**
		HZS	78	**-4.4×10^{-4}**	**5.60**	**<0.001**	**0.29**	**-7.8×10^{-4}**	**4.84**	**<0.001**	**0.23**
Mean proportional pool length	Pool lengths, riffle ER	LZS	77	4.3×10^{-8}	0.11	0.91	<0.01	**-3.8×10^{-3}**	**15.5**	**<0.001**	**0.76**
		HZS	77	**-3.5×10^{-4}**	**4.29**	**<0.001**	**0.19**	**-4.6×10^{-3}**	**8.46**	**<0.001**	**0.48**
Mean proportional riffle length	Riffle lengths	LZS	77	-7.3×10^{-8}	0.78	0.44	0.01	8.2×10^{-6}	0.88	0.38	<0.01
		HZS	77	**1.4×10^{-4}**	**3.73**	**<0.001**	**0.15**	1.3×10^{-6}	1.88	0.06	0.04
ER density measures											
ER density	Riffle ER, pool ER	LZS	78	-3.3×10^{-9}	0.19	0.85	<0.01	-1.3×10^{-6}	0.70	0.49	<0.01
		HZS	78	-1.3×10^{-5}	0.49	0.63	<0.01	7.1×10^{-5}	0.83	0.41	<0.01
Mean density of riffle ER	Riffle ER	LZS	78	-4.1×10^{-8}	1.37	0.18	0.02	**-1.1×10^{-4}**	**12.3**	**<0.001**	**0.66**
		HZS	78	-5.1×10^{-5}	1.26	0.21	0.02	**-4.2×10^{-4}**	**5.02**	**<0.001**	**0.24**
Mean density of riffle ER	Pool lengths, riffle ER	LZS	77	-9.1×10^{-9}	0.30	0.77	<0.01	**-3.2×10^{-4}**	**22.4**	**<0.001**	**0.87**
		HZS	77	**-8.9×10^{-5}**	**3.28**	**0.002**	**0.12**	**-1.9×10^{-3}**	**17.1**	**<0.001**	**0.79**
Pool-riffle ER density ratio	Riffle ER	LZS	78	-2.0×10^{-5}	1.00	0.32	0.01	**0.075**	**11.9**	**<0.001**	**0.64**
		HZS	78	-8.1×10^{-3}	0.90	0.37	0.01	**0.093**	**4.97**	**<0.001**	**0.24**
Pool-riffle ER density ratio	Pool lengths, riffle ER	LZS	77	-7.6×10^{-7}	0.04	0.97	<0.01	**0.19**	**13.3**	**<0.001**	**0.69**
		HZS	77	**3.1×10^{-2}**	**5.11**	**<0.001**	**0.25**	**0.38**	**9.71**	**<0.001**	**0.55**
Segments without ER											
Number of segments without ER	Pool lengths	HZS	78	**-7.8×10^{-4}**	**9.93**	**<0.001**	**0.03**	**-1.2×10^{-3}**	**6.18**	**<0.001**	**0.33**
Maximum length without ER	Pool lengths	HZS	78	**-3.4×10^{-3}**	**5.70**	**<0.001**	**0.29**	-1.8×10^{-3}	1.29	0.20	0.02

Note. t-tests indicate whether slopes differ from zero, significant tests are shown in bold text.

Script S1.

R scripts for calculating fractal dimensions

```
# Functions for calculating 1D fractal dimensions
################################

#References:
#########
# fractaldim:::IsInBox function from fractaldim library
library(ggpmisc)
library(stats)
library(lmodel2)
library(plyr)

##Box Counting Functions
#################

## IsInBox
IsInBoxBC <- function (IsInBoxdata, boxx, boxy)
{
 IsInBoxdata <- subset(IsInBoxdata, IsInBoxdata[,1]>= boxx[1])
 IsInBoxdata <- subset(IsInBoxdata, IsInBoxdata[,1]<= boxx[2])
 if (nrow(IsInBoxdata)>0){
  for (i in 1:nrow(IsInBoxdata))
  { if(any((IsInBoxdata[i,2] >= boxy[1]) & (IsInBoxdata[i,2] <= boxy[2])))
  {return(TRUE)}} }
 return(FALSE)
}

## CrossingBox
CrossingBoxyBC <- function (Crossdata, boxx, boxy)
{
 Crossdata <- subset(Crossdata, Crossdata[,1]>= boxx[1])
 Crossdata <- subset(Crossdata, Crossdata[,1]<= boxx[2])
 Add <- 0
 nrow(Crossdata)
 if (nrow(Crossdata)>0){
  for (j in 1:nrow(Crossdata))
  { if(Crossdata[j,2] >= boxy[2]) {Add <- 1}}
 }
 return(Add)
}

CrossingBoxxBC <- function (Crossdata, boxx, boxy)
{
 Crossdata <- subset(Crossdata, Crossdata[,2]>= boxy[1])
 Crossdata <- subset(Crossdata, Crossdata[,2]<= boxy[2])
```

```
  Add <- 0

  if (nrow(Crossdata)>0){
   for (k in 1:nrow(Crossdata))
   { if(Crossdata[k,1] >= boxx[2]) {Add <- 1}}

  }
  return(Add)
}

CrossingBoxxyBC <- function (Crossdata, boxx, boxy)
{
  Crossdata <- subset(Crossdata, Crossdata[,1]>= boxx[2])
  Crossdata <- subset(Crossdata, Crossdata[,2]>= boxy[2])
  Add <- 0
  if(nrow(Crossdata) < 0) {Add <- 1}
  return(Add)
}

## BoxCount
BoxCount_Fun <- function (data, numcases, boxsize, data.range.x, data.range.y)
{
  Ninternal <- 0
  width <- boxsize
  height <- boxsize

  minboxx <- data.range.x[1]
  minboxy <- data.range.y[1]
  maxboxx <- data.range.x[2]
  maxboxy <- data.range.y[2]

  qh <- trunc(maxboxx/width)
  qv <- max(trunc(maxboxy/height),1)

  for (hor in 1:qh) {
   boxxlimits <- c((min(data[,1]) + (hor-1) * width),(min(data[,1]) + (hor) * width))

   for (ver in 1:qv) {
    boxylimits <- c((min(data[,2]) + (ver-1) * height), (min(data[,2]) + ver * height))

    if(IsInBoxBC(data, boxxlimits, boxylimits))
    {Ninternal <- Ninternal + 1}

    if(hor == qh) {
     Addx <- CrossingBoxxBC(data, boxxlimits, boxylimits)
     Ninternal <- Ninternal + Addx }

    if(ver == qv){
```

```
    Addy <- CrossingBoxyBC(data, boxxlimits, boxylimits)
    Ninternal <- Ninternal + Addy }
  }

  Addxy <- CrossingBoxxyBC(data, boxxlimits, boxylimits)
  Ninternal <- Ninternal + Addxy
 }
 return(Ninternal)
}

## Run Box-counting functions
Function_Run_Box_Counting <- function(Delta = TRUE) {
 library(plyr)
 if("Rocks" %in% colnames(data1D)){
  # 1D data:
  data <- subset(data1D, Rocks > 0)
  data <- uncount(data = data, weights = data$Rocks)
  data$Y..m. <- 1
  data$X..m. <- data$X_coord
  min_box_size <- 5
  decimal_places <- 0

 }else{
  # 2D data:
  data <- data1D
  min_box_size <- 0.2
  decimal_places <- 2
 }

 Rivers <-as.character(unique(data$River))

 boxcount_results_lm1 <- array(0, dim = c(length(Rivers), 4))
 boxcount_results_lm2 <- array(0, dim = c(length(Rivers), 4))
 Delta2onwards_LIST <- list()
 DELTAS <- data.frame(River = Rivers, new_delta = vector("numeric",length(Rivers)))
 Snipping_values <- data.frame(River = Rivers, pointsremove =
vector("numeric",length(Rivers)))

 for (g in 1:length(Rivers)) {
  data2D_format <- data[data$River==Rivers[g],]
  data2D_format <- subset(data2D_format, select = c(X..m.,Y..m.))

  n <- nrow(data2D_format)
  data.range.x <- range(data2D_format[1:n,1])
  data.range.y <- range(data2D_format[1:n,2])
  sizes <- round(seq(from = data.range.x[1], to = data.range.x[2], by = min_box_size), digits =
decimal_places)
  sizes <- sizes[sizes != 0]
```

```
  delta <- length(sizes)
  neff <- trunc((n - 1)/((delta - 1)*5)) * ((delta - 1)*5) + 1
  Box <- array(0,c(delta,3))

  for (a in (1:delta)) {
   Box[a,1] <- sizes[a]
   Box[a,2] <- log(BoxCount_Fun(data = data2D_format, numcases = neff, boxsize = sizes[a],
data.range.x, data.range.y))
   Box[a,3] <- a
  }
  colnames(Box) <- c("delta", "log_boxcount", "old_delta")

  Box <- as.data.frame(Box[!duplicated(Box[,2]), ])
  Box <- as.data.frame(Box[1:nrow(Box)-1, ])

  Delta2onwards_LIST[[g]]<- Box
  DELTAS$new_delta[g] <- nrow(Box)
  Snipping_values$pointsremove[g] <- nrow(Box)

  Delta2onwardsdf <- as.data.frame(Box)
  lm <- lm(log_boxcount~log(delta), data=Delta2onwardsdf)
  boxcount_results_lm1[g,1:4] <- rbind(as.character(Rivers[g]),
as.numeric(summary(lm)$coefficients[2]), summary(lm)$coefficients[1],
summary(lm)$r.squared)

  lm2 <- lmodel2(Delta2onwardsdf$log_boxcount~log(Delta2onwardsdf$delta),
data=Delta2onwardsdf)
  lm2_intercept <- lm2$regression.results[3,2] # print intercept
  lm2_slope <- lm2$regression.results[3,3] # print slope
  lm2_rsquare <- lm2$rsquare # print R2

  boxcount_results_lm2[g,1:4] <- rbind(as.character(Rivers[g]), lm2_slope, lm2_intercept,
lm2_rsquare)
  rm(delta, g, data2D_format)

 }

 names(Delta2onwards_LIST) <- Rivers
 colnames(boxcount_results_lm1) <- c("River", "lm1_slope", "lm1_Intercept", "R_squared")
 colnames(boxcount_results_lm2) <- c("River", "lm2_slope", "lm2_Intercept", "R_squared")
 boxcount_LM_results <- cbind(as.data.frame(boxcount_results_lm1),
as.data.frame(boxcount_results_lm2[,2:4]))

 # Output:
 List_boxcount <- list()
 List_boxcount$boxcount_LM_results <- boxcount_LM_results
 List_boxcount$Delta2onwards_LIST <- Delta2onwards_LIST
 List_boxcount$DELTAS <- DELTAS
```

```
  List_boxcount$Snipping_values <- Snipping_values

  return(List_boxcount)

}

##Entropy Functions
##############

## IsInBox
IsInBoxE <- function (IsInBoxdata, boxx, boxy)
{
  IsInBoxdata <- subset(IsInBoxdata, IsInBoxdata[,1]>= boxx[1])
  IsInBoxdata <- subset(IsInBoxdata, IsInBoxdata[,1]<= boxx[2])

  Add <- 0
  if (nrow(IsInBoxdata)>0){
    for (i in 1:nrow(IsInBoxdata))
    { if(any((IsInBoxdata[i,2] >= boxy[1]) & (IsInBoxdata[i,2] <= boxy[2])))
    {Add <- Add + 1}} }
  Add
  return(Add)
}

## CrossingBox
CrossingBoxyE <- function (Crossdata, boxx, boxy)
{

  Crossdata <- subset(Crossdata, Crossdata[,1]>= boxx[1])
  Crossdata <- subset(Crossdata, Crossdata[,1]<= boxx[2])
  Add <- 0
  nrow(Crossdata)

  if (nrow(Crossdata)>0){
    for (j in 1:nrow(Crossdata))
    { if(Crossdata[j,2] >= boxy[2]) {Add <- Add + 1}}

  }
  Add
  return(Add)
}

CrossingBoxxE<- function (Crossdata, boxx, boxy)
{
  Crossdata <- subset(Crossdata, Crossdata[,2]>= boxy[1])
  Crossdata <- subset(Crossdata, Crossdata[,2]<= boxy[2])
  Add <- 0
```

```
 if (nrow(Crossdata)>0){
  for (k in 1:nrow(Crossdata))
  { if(Crossdata[k,1] >= boxx[2]) {Add <- Add + 1}}

 }
 return(Add)
}

CrossingBoxxyE <- function (Crossdata, boxx, boxy)
{
 Crossdata <- subset(Crossdata, Crossdata[,1]>= boxx[2])
 Crossdata <- subset(Crossdata, Crossdata[,2]>= boxy[2])
 Add <- 0
 if(nrow(Crossdata) < 0) {Add <- Add + 1}
 return(Add)
}

## Entropy
Entropy_Fun <- function (data, numcases, boxsize, data.range.x, data.range.y)
{

 width <- boxsize
 height <- boxsize
 minboxx <- data.range.x[1]
 minboxy <- data.range.y[1]
 maxboxx <- data.range.x[2]
 maxboxy <- data.range.y[2]

 qh <- trunc(maxboxx/width)
 qv <- trunc(maxboxy/height)
 if(qv < 1) {qv <- 1}

 # Calculate the total number of rocks
 CountRocks <- array(0, dim = c(max(1,qh),  max(1,qv)))

 for (hor in 1:qh) {
  boxxlimits <- c((min(data[,1]) + (hor-1) * width),(min(data[,1]) + (hor) * width))
  boxxlimits

  for (ver in 1:qv) {
   boxylimits <- c((min(data[,2]) + (ver-1) * height), (min(data[,2]) + ver * height))
   boxylimits

   Addbase <- IsInBoxE(data, boxxlimits, boxylimits)
   CountRocks[hor,ver] <- Addbase
  }
 }
 CountRocks
```

```
 sum(CountRocks)

 # Calculate weighted pi
 pivalues <- array(0, dim = c(nrow(CountRocks),ncol(CountRocks)))
 pilogpivalues <- array(0, dim = c(nrow(CountRocks),ncol(CountRocks)))

 TotalRocks <- sum(CountRocks)

 for (m in 1:nrow(CountRocks))
 {
  for (l in 1:ncol(CountRocks))
  {
   if(CountRocks[m,l] > 0)
   {
    pivalues[m,l] <- CountRocks[m,l] / TotalRocks
    pilogpivalues[m,l] <- pivalues[m,l] * log(pivalues[m,l])
   }
  }
 }

 Hdelta <- -sum(pilogpivalues)

 # Correct for bias in the estimate of entropy as per Basharin (1959)
 Samplesize <- length(CountRocks)
 Hdeltaunbiased <- Hdelta + ((Samplesize - 1)/(2 * TotalRocks)*(log2(exp(1))))
 return(Hdeltaunbiased)
}

## Run Entropy functions
Function_Run_Entropy <- function (Delta = TRUE) {
 library(plyr)
 if("Rocks" %in% colnames(data1D)){
  #1D data:
  data <- subset(data1D, Rocks > 0)
  data <- uncount(data = data, weights = data$Rocks)
  data$Y..m. <- 1
  data$X..m. <- data$X_coord
  min_box_size <- 5
  decimal_places <- 0

 }else{
  #2D data:
  data <- data1D
  min_box_size <- 0.2
  decimal_places <- 2
 }

 Rivers <-as.character(unique(data$River))
```

```
  Delta2onwards_LIST <- list()
  DELTAS <- data.frame(River = Rivers, new_delta = vector("numeric",length(Rivers)))
  Snipping_values <- data.frame(River = Rivers, pointsremove =
vector("numeric",length(Rivers)))

  for (g in 1:length(Rivers)) {
    data2D_format <- data[data$River==Rivers[g],]
    data2D_format <- subset(data2D_format, select = c(X..m.,Y..m.))

    n <- nrow(data2D_format)
    data.range.x <- range(data2D_format[1:n,1])
    data.range.y <- range(data2D_format[1:n,2])
    sizes <- round(seq(from = data.range.x[1], to = data.range.x[2], by = min_box_size), digits =
decimal_places)
    sizes <- sizes[sizes != 0]
    delta <- length(sizes)
    neff <- trunc((n - 1)/((delta - 1)*5)) * ((delta - 1)*5) + 1

    Entropy <- array(0,c(delta,5))
    for (a in (1:delta)) {  #a<-1
      Entropy[a,1] <- sizes[a]
      Entropy[a,5] <- Entropy_Fun(data = data2D_format, numcases = neff, boxsize = sizes[a],
data.range.x, data.range.y)
      Entropy[a,2] <- log(Entropy[a,5])
      Entropy[a,3] <- a
      Entropy[a,4] <- round(Entropy[a,5], digits = 1)
    }
    colnames(Entropy) <- c("delta", "log_Entropy", "old_delta", "Round_Entropy",
"Entropy_Unlogged")

    Entropy <- as.data.frame(Entropy[!duplicated(Entropy[,4]), ])
    Entropy <- as.data.frame(Entropy[1:nrow(Entropy)-1, ])

    Delta2onwards_LIST[[g]]<- Entropy
    DELTAS$new_delta[g] <- nrow(Entropy)
    Snipping_values$pointsremove[g] <- nrow(Entropy)

    rm(delta, g, data2D_format)

  }

  names(Delta2onwards_LIST) <- Rivers

  # Ouputs:
  List_Entropy <- list()
  List_Entropy$Delta2onwards_LIST <- Delta2onwards_LIST
  List_Entropy$DELTAS <- DELTAS
  List_Entropy$Snipping_values <- Snipping_values
```

```
  return(List_Entropy)

}

# Function for Log-transformed linear regression of delta vs NX
########################################

## Log-Log regression
Function_FDSlope <- function() {

  Rivers <- unique(data1D$River)
  FDSlope_results <- data.frame(River = Rivers, Intercept= vector("numeric",length(Rivers)),
Slope = vector("numeric",length(Rivers)), R2 = vector("numeric",length(Rivers))) #NULL

  for (g in 1:length(Rivers)) {
    Delta2onwards <- as.data.frame(Delta2onwards_LIST[[g]])

   # Log-Log Plot
    Plot <- ggplot(Delta2onwards, aes(x= log(Delta2onwards$delta), y = Delta2onwards[,2])) +
      geom_point(size = 3) +
      xlab(expression(log(delta))) + ylab(expression(log(N["X"]))) +
      ggtitle(as.character(Rivers[g]))+
      theme_bw()+ theme(text = element_text(size=15), axis.text = element_text(size=15),
legend.position = "none", panel.grid = element_blank()) +
      stat_smooth(method="lm", se=FALSE)+
      stat_poly_eq(formula = y ~ x, aes(label = paste(..eq.label.., ..rr.label.., sep = "~~~")), parse =
TRUE, label.y = "top", label.x = "right")

    print(Plot)

    #Extract intercept, slope, and R-squared from lm()
    river_lm <- lm(Delta2onwards[,2] ~ log(Delta2onwards$delta))
    FDSlope_results$Intercept[g] <- summary(river_lm)$coefficients[1]
    FDSlope_results$Slope[g] <- summary(river_lm)$coefficients[2]
    FDSlope_results$R2[g] <- summary(river_lm)$r.squared
  }
  return(FDSlope_results)
}

# Function for the R² - SSR Procedure
########################

## R2SSR
Function_R2SSR <- function() {
  Rivers <- unique(data1D$River)
  R2SSR_results <- data.frame(River = Rivers, R2SSR_FD = vector("numeric",length(Rivers)),
R2SSR_test_result = vector("logical",length(Rivers))) #NULL
```

```
 for (g in 1:length(Rivers)) {
  delta <- DELTAS[g,2]
  Plotdataframe <- as.data.frame(Delta2onwards_LIST[[g]])
  windowsize <- 6 #smallest window size
  iterations <- 0
  for (j in windowsize:(delta-1))
  {
   iterations <- iterations + (delta - (j))
  }

  R2SSR <- array(0, dim = c((iterations), 4))
  colnames(R2SSR) <- c("Rsquared", "SSR", "Slope", "Iterations")
  startlocation <- 1

  for (k in 1:iterations)
  {
   Residualcalc <- array(0, dim = c(windowsize,6))

   # Standard major axis regression
   R2SSRlm <- lmodel2(Plotdataframe[startlocation:(windowsize+startlocation-1),2] ~
log(Plotdataframe[startlocation:(windowsize+startlocation-1),1]), data = Plotdataframe)

   # Calculate sum of squared residuals and R2
   SMAslope <- R2SSRlm$regression.results[3,3]
   SMAintercept <- R2SSRlm$regression.results[3,2]

   for (i in 1:nrow(Residualcalc))
   {
    Residualcalc[i,1] <- log(Plotdataframe[(startlocation+i-1),1])
    Residualcalc[i,2] <- Plotdataframe[(startlocation+i-1),2]
    Residualcalc[i,3] <- SMAslope * Residualcalc[i,1] + SMAintercept
    Residualcalc[i,4] <- Residualcalc[i,3] - Residualcalc[i,2]
    Residualcalc[i,5] <- Residualcalc[i,4]^2
    Residualcalc[i,6] <- Residualcalc[i,1]*Residualcalc[i,2]
   }

   SSRSMA <- sum(Residualcalc[,5])
   TotalSS <- sum(Residualcalc[,2]^2) - ((sum(Residualcalc[,2])^2)/nrow(Residualcalc))
   RegressionSS <- (((sum(Residualcalc[,6]))-
((sum(Residualcalc[,1])*sum(Residualcalc[,2]))/nrow(Residualcalc)))^2)/(sum(Residualcalc[,1]^2
)-((sum(Residualcalc[,1])^2/nrow(Residualcalc))))
   R2SMA <- RegressionSS / TotalSS
   R2SSR[k,2] <- SSRSMA
   R2SSR[k,1] <- R2SMA
   R2SSR[k,3] <- SMAslope
   R2SSR[k,4] <- k+1
```

```
    if (startlocation < ((delta)-(windowsize)))
    {
      (startlocation <- startlocation + 1)
    } else
    {
      startlocation <- 1
      windowsize <- windowsize + 1
    }
  }

  # Output:
  R2SSR <- as.data.frame(R2SSR)
  R2SSR_test_result <- which.min(R2SSR[,2]) == which.max(R2SSR[,1])
  R2SSR_FD <- as.numeric(abs(R2SSR[which.min(R2SSR[,2]),3]))

  R2SSR_results[g,2] <- R2SSR_FD
  R2SSR_results[g,3] <- R2SSR_test_result

  ggplot(R2SSR, aes(x= SSR, y= Rsquared))+
    geom_point(size = 3, shape = 21) +
    geom_point(data = R2SSR[R2SSR$Rsquared == max(R2SSR$Rsquared),], alpha = 0.5, colour
= "red", size = 3) +
    geom_point(data = R2SSR[R2SSR$SSR == min(R2SSR$SSR),], alpha = 0.5, colour = "blue",
size = 3) +
    ggtitle(as.character(Rivers[g]))+
    ylab(expression(R^2)) + xlab("SSR") +
    theme_bw()+ theme(text = element_text(size=15), axis.text = element_text(size=15),
legend.position = "none", panel.grid = element_blank())

 }
 return(R2SSR_results)
}


# Function for the Zero Slope Procedure
###########################

## Zero Slope
Function_Zero_Slope <- function() {
 Rivers <- unique(data1D$River)
 Zero_Slope_results <- data.frame(River = Rivers, Optintercept =
vector("numeric",length(Rivers)), ZeroSlope_test_result = vector("logical",length(Rivers)),
ZeroSlope_Lower = vector("logical",length(Rivers)), ZeroSlope_Upper =
vector("logical",length(Rivers))) #NULL

 for (g in 1:length(Rivers)) {
  delta <- DELTAS$new_delta[g]
  Plotdataframe <- as.data.frame(Delta20nwards_LIST[[g]][1:delta,])
```

```
Independentz <- log(Plotdataframe[,1])
Dependentz <- Plotdataframe[,2]

deriv <- function(x, y) diff(y) / diff(x)
middle_pts <- function(x) x[-1] - diff(x) / 2
first_d <- deriv(Independentz, Dependentz)
Independentza <- middle_pts(Independentz)

iterationz <- 0
minwindowsize <- 6

for (j in minwindowsize:(delta-1))   # 6 is the minimum window size
{
 iterationz <- iterationz + (delta - (j+1))
}

Zeroslopez <- array(0, dim = c((iterationz),4))
colnames(Zeroslopez) <- c("F", "p", "windowsize", "startinglocation")
startlocationz <- 1
windowsizez <- minwindowsize

for (k in 1:iterationz)
{
 Residualcalcz <- array(0, dim = c(windowsizez,6))

 NewDependentz <- first_d[startlocationz:(windowsizez+startlocationz-1)]
 NewIndependentz <- Independentza[startlocationz:(windowsizez+startlocationz-1)]

 # Standard major axis regression
 R2SSRlmz <- lmodel2(NewDependentz ~ NewIndependentz)
 Zslopez <- R2SSRlmz$regression.results[3,3]
 Zerointerceptz <- R2SSRlmz$regression.results[3,2]

 for (i in 1:nrow(Residualcalcz))
 {
  Residualcalcz[i,1] <- NewIndependentz[i]
  Residualcalcz[i,2] <- NewDependentz[i]
  Residualcalcz[i,3] <- Zslopez * Residualcalcz[i,1] + Zerointerceptz
  Residualcalcz[i,4] <- Residualcalcz[i,3] - Residualcalcz[i,2]
  Residualcalcz[i,5] <- Residualcalcz[i,4]^2
  Residualcalcz[i,6] <- Residualcalcz[i,1]*Residualcalcz[i,2]
 }

 SSRSMAz <- sum(Residualcalcz[,5])
 TotalSSz <- sum(Residualcalcz[,2]^2) - ((sum(Residualcalcz[,2])^2)/nrow(Residualcalcz))
 RegressionSSz <- (((sum(Residualcalcz[,6]))-
((sum(Residualcalcz[,1])*sum(Residualcalcz[,2]))/nrow(Residualcalcz)))^2)/(sum(Residualcalcz[,
1]^2)-((sum(Residualcalcz[,1])^2/nrow(Residualcalcz))))
```

```
  R2SMAz <- RegressionSSz / TotalSSz

  RegressionMSz <- RegressionSSz / 1
  ResidualMSz <- (TotalSSz - RegressionSSz)/(nrow(Residualcalcz)-2)
  Zeroslopez[k,1] <- RegressionMSz/ResidualMSz
  Zeroslopez[k,2] <- pf(Zeroslopez[k,1], df1=1, df2=(nrow(Residualcalcz)-2), lower.tail=FALSE)
  Zeroslopez[k,3] <- windowsizez
  Zeroslopez[k,4] <- startlocationz

  if (startlocationz < ((delta-1)-(windowsizez)))
  {
   (startlocationz <- startlocationz + 1)
  } else
  {
   startlocationz <- 1
   windowsizez <- windowsizez + 1
  }
 }

 # calculate the number of regression windows that have a slope significantly different from
zero
 length(Zeroslopez[,2])
 sum(Zeroslopez[,2] < 0.05)
 z_insig_results <- as.data.frame(subset(Zeroslopez, Zeroslopez[,2] > 0.05))
 ZeroSlope_pass <- nrow(z_insig_results)>0
 zeroslopez_largest <- z_insig_results[length(z_insig_results$windowsize),]

 # Finding the confidence intervals for the ZERO slope lines for the window of interest by
bootstrapping the entropy values
 nruns <- 100
 Critwindowsize <- 6
 Critstartlocation <- 1

 critdelta<- Critstartlocation + Critwindowsize -1
 BootFDZ <-  array(0,dim = c(nruns,1))

 for (m in 1:nruns)
 {
  PlotdataCIz <- array(0, dim = c(delta, 2))
  colnames(PlotdataCIz) <- c("delta", "entropy")

  SelectedEntropy <- sample(1:nrow(Plotdataframe), delta, replace = TRUE)

  for (j in 1:delta)
  {
   PlotdataCIz[j,2] <- Plotdataframe[SelectedEntropy[j],2]
  }
```

```
    PlotdataCIz[,1] <- Plotdataframe[,1]
    PlotdataCIz[,2] <- sort(PlotdataCIz[,2], decreasing = TRUE)

    # calculate the zero slope
    IndependentCIz <- log(PlotdataCIz[,1])
    DependentCIz <- PlotdataCIz[,2]

    first_dCI <- deriv(IndependentCIz, DependentCIz)
    IndependentzCIa <- middle_pts(IndependentCIz)
    NewDependentCIz <- first_dCI
    NewIndependentCIz <- IndependentzCIa

    R2SSRlmbootz <- lm(NewDependentCIz ~ 1 + offset(0 * NewIndependentCIz))
    BootFDZ[m] <- summary(R2SSRlmbootz)$coefficients[1,1]
  }

  # find the 2.5th and 97.5th percentiles (95% confidence intervals)
  BootFDZ <- sort(BootFDZ)
  LowerScatterZ <- BootFDZ[nruns/40]
  UpperScatterZ <- BootFDZ[39*nruns/40]

  # Find the optimal intercept
  OptDependentz <- first_d
  OptIndependentz <- Independentza

  R2SSRlmoptz <- lm(OptDependentz ~ 1 + offset(0 * OptIndependentz))
  Optintercept <- summary(R2SSRlmoptz)$coefficients[1,1]
  OptSig <- summary(R2SSRlmoptz)$coefficients[1,4]<0.05

  zero_slope_data <- as.data.frame(OptIndependentz)
  zero_slope_data$OptDependentz <- OptDependentz

  # Outputs:
  ggplot(zero_slope_data, aes(x= OptIndependentz, y= OptDependentz))+
    geom_point(size = 3, shape = 21) +
    geom_hline(yintercept = Optintercept, colour = "red") +
    geom_hline(yintercept = LowerScatterZ, colour = "blue", linetype="dashed") +
    geom_hline(yintercept = UpperScatterZ, colour = "blue", linetype="dashed") +
    ylim(-10,2) +
    ggtitle(as.character(Rivers[g]))+
    xlab(expression(log(delta))) + ylab(expression(~italic(d)~log(N[B]))) +
    theme_bw()+ theme(text = element_text(size=15), axis.text = element_text(size=15),
legend.position = "none", panel.grid = element_blank())

  z_insig_results <- as.data.frame(subset(Zeroslopez, Zeroslopez[,2] > 0.05))
  ZeroSlope_pass <- nrow(z_insig_results)>0
  Zero_Slope_results[g,2] <- Optintercept
  Zero_Slope_results[g,3] <- OptSig
```

```
    Zero_Slope_results[g,4] <- LowerScatterZ
    Zero_Slope_results[g,5] <- UpperScatterZ
  }
  return(Zero_Slope_results)
}

# Function for the Compensated-slope Procedure
################################
## Compensated-slope
Function_Compensated_Slope <- function() {
  nCvalues <- 101
  Rivers <- unique(data1D$River)
  Compensated_Slope_results <- data.frame(River = Rivers, Cvalue =
vector("numeric",length(Rivers)), C_slope_MIn = vector("logical",length(Rivers)), C_slope_Max
= vector("logical",length(Rivers)), C_slope_MIn2 = vector("logical",length(Rivers)),
C_slope_Max2 = vector("logical",length(Rivers)))

  for (g in 1:length(Rivers)) {
    delta        <- DELTAS$new_delta[g]        # delta <- 20
    Plotdataframe <- as.data.frame(Delta20nwards_LIST[[g]][1:delta,])
    FDvalue      <- abs(FDSlope_results$Slope[g])

    Cvalues <- seq(0, FDvalue+1, length= nCvalues)

    # calculate constant k based on M(delta) = log k x DF log delta
    CalcFD <- array(0, dim = c(nrow(Plotdataframe), 3))
    CalcFD[,1] <- Plotdataframe[,1]
    CalcFD[,2] <- Plotdataframe[,2]
    kconstant <- mean(exp(CalcFD[,2] + FDvalue * log(CalcFD[,1])))
    CalcFD[,3] <- (log(kconstant)- CalcFD[,2])/ log(CalcFD[,1])
    colnames(CalcFD) <-(c("delta", "entropy", "FD value"))

    iterationc <- 0
    for (j in 6:(delta))   # 6 is the minimum window size
    {
      iterationc <- iterationc + (delta - (j))
    }

    Compslopec <- array(0, dim = c((iterationc),3, length(Cvalues)))
    colnames(Compslopec) <- c("F", "p", "cvalue")

    startlocationc <- 1
    windowsizec <- 6

    for (k in 1:iterationc)
    {
      Residualcalcc <- array(0, dim = c(windowsizec, 6, length(Cvalues)))
      for (b in 1:length(Cvalues))
```

```
    {
     Independentc <- log(CalcFD[startlocationc:(windowsizec+startlocationc-1),1])
     Dependentc <- log((CalcFD[startlocationc:(windowsizec+startlocationc-1),1] ^ Cvalues[b]) *
(CalcFD[startlocationc:(windowsizec+startlocationc-1),1] ^ -
CalcFD[startlocationc:(windowsizec+startlocationc-1),3]))

     R2SSRlmc <- lmodel2(Dependentc ~ Independentc)
     Cslopec <- R2SSRlmc$regression.results[3,3]
     Compinterceptc <- R2SSRlmc$regression.results[3,2]

     for (i in 1:nrow(Residualcalcc))
     {
      Residualcalcc[i,1,b] <- Independentc[i]
      Residualcalcc[i,2,b] <- Dependentc[i]
      Residualcalcc[i,3,b] <- Cslopec * Residualcalcc[i,1,b] + Compinterceptc
      Residualcalcc[i,4,b] <- Residualcalcc[i,3,b] - Residualcalcc[i,2,b]
      Residualcalcc[i,5,b] <- Residualcalcc[i,4,b]^2
      Residualcalcc[i,6,b] <- Residualcalcc[i,1,b]*Residualcalcc[i,2,b]
     }

     SSRSMAc <- sum(Residualcalcc[,5,b])
     TotalSSc <- sum(Residualcalcc[,2,b]^2) - ((sum(Residualcalcc[,2,b])^2)/nrow(Residualcalcc))
     RegressionSSc <- (((sum(Residualcalcc[,6,b]))-
((sum(Residualcalcc[,1,b])*sum(Residualcalcc[,2,b]))/nrow(Residualcalcc)))^2)/(sum(Residualca
lcc[,1,b]^2)-((sum(Residualcalcc[,1,b])^2/nrow(Residualcalcc))))
     R2SMAc <- RegressionSSc / TotalSSc
     R2SMAc

     RegressionMSc <- RegressionSSc / 1
     ResidualMSc <- (TotalSSc - RegressionSSc)/(nrow(Residualcalcc)-2)
     Compslopec[k,1,b] <- RegressionMSc/ResidualMSc
     Compslopec[k,2,b] <- pf(Compslopec[k,1,b], df1=1, df2=(nrow(Residualcalcc)-2),
lower.tail=FALSE)
     Compslopec[k,3,b] <- Cvalues[b]
    }

    if (startlocationc < (delta-(windowsizec)))
    {
     (startlocationc <- startlocationc + 1)
    } else
    {
     startlocationc <- 1
     windowsizec <- windowsizec + 1
    }
   }

  RevisedCompslopec <- array(0, dim = c(length(Cvalues),3))
  colnames(RevisedCompslopec) <- c("F", "p", "cslope")
```

```
  Compslopec[,,b]
  for (xx in 1:length(Cvalues))
  {
    RevisedCompslopec[xx,1] <- Compslopec[iterationc,1,xx]
    RevisedCompslopec[xx,2] <- Compslopec[iterationc,2,xx]
    RevisedCompslopec[xx,3] <- Compslopec[iterationc,3,xx]
  }
  FD_iteration <- which(RevisedCompslopec[,2] == max(RevisedCompslopec[,2]))

  # Plot
  par(mar = c(5.1, 4.5, 4.1, 1))
  plot(log(CalcFD[,1]), log((CalcFD[,1] ^ Cvalues[1]) * (CalcFD[,1] ^ -CalcFD[,3])), ylim = c(-8,10),
      xlab = expression(log(delta)),
      ylab = expression(paste("log(", delta^C, " ",x, " ",delta^-D[X],")")),
      main = as.character(Rivers[g]))
  for (i in 2:nCvalues)
  {  points(log(CalcFD[,1]), log((CalcFD[,1] ^ Cvalues[(i)]) * (CalcFD[,1] ^ -CalcFD[,3])), col =
(i+1))
  }
  points(log(CalcFD[,1]), log((CalcFD[,1] ^ Cvalues[(FD_iteration)]) * (CalcFD[,1] ^ -CalcFD[,3])),
col = "black", pch = 19)
  Compensated_Slope_results[g,2] <- Cvalues[FD_iteration]

  Comp_slope_CI_results <- data.frame()
  for (i in 1:nCvalues)
  {
    Comp_slope_CI_results[i,1] <-Cvalues[i]
    Comp_slope_CI_results[i,2] <-Compslopec[iterationc,2,i]
    Comp_slope_CI_results[i,3] <-Compslopec[1,2,i] <0.05
    Comp_slope_CI_results[i,4] <-length(which(Compslopec[,2,i] >= 0.05))
    Comp_slope_CI_results[i,5] <-length(which(Compslopec[,2,i] >=
0.05))/length(Compslopec[,2,i])
    Comp_slope_CI_results[i,6] <-Compslopec[iterationc,2,i]
  }
  colnames(Comp_slope_CI_results) <- c("Cvalues", "p", "Significant", "N_Significant",
"PER_Significant", "LAST_VALUE_SIG")

  CI_Range<- Comp_slope_CI_results[Comp_slope_CI_results$PER_Significant > 0,]
  CI_Range2<- Comp_slope_CI_results[Comp_slope_CI_results$LAST_VALUE_SIG > 0.05,]
  Compensated_Slope_results[g,3] <- min(CI_Range[,1])
  Compensated_Slope_results[g,4] <- max(CI_Range[,1])
  Compensated_Slope_results[g,5] <- min(CI_Range2[,1])
  Compensated_Slope_results[g,6] <- max(CI_Range2[,1])
 }

 return(Compensated_Slope_results)
}
```

Script S2.

R scripts for simulating synthetic stream stretches

```
#Simulate 1D synthetic stream stretches
##########################

#Packages required:
#############
library(dplyr)
library(ggplot2)

# Function to generate Pool-Riffle sequence:
############################
# Generates Riffle and Pool lengths using distrubutions of riffle and pool lengths from
# Australian and Scottish study streams.
# With ability to manipulate either riffle or pool lengths.
RP_sequence <- function(River_length = 1000,
                PL_meanlog = 1.3715, PL_sdlog = 0.5711,
                RL_meanlog = 2.0488, RL_sdlog = 0.8286,
                PL_multiplier = 1, RL_multiplier = 1
){
 n <- River_length/5
 P_lengths <- round(rlnorm(n = n, meanlog = PL_meanlog, sdlog = PL_sdlog)*PL_multiplier)
#POOLS   #0
 R_lengths <- round(rlnorm(n = n, meanlog = RL_meanlog, sdlog = RL_sdlog)*RL_multiplier)
#Riffles  #1

 #Translate these lengths in to sequences of 1s and 0s for riffle and pool segments:
 PR0 <- as.numeric()
 for (j in 1:n) {
  PR1 <- c(rep(0, P_lengths[j]), rep(1,R_lengths[j]))  #Pools = 0, Riffles = 1
  PR0 <- c(PR0,PR1)
 }

 PR0 <- PR0[1:(River_length/5)]

 #Prepare output:
 RP_10_sequence_data <- list()
 RP_10_sequence_data$Sequence <- PR0
 RP_10_sequence_data$P_lengths <- P_lengths
 RP_10_sequence_data$R_lengths <- R_lengths

 RP_10_sequence_data
}
```

```
# Function to simulate ER counts:
########################
#Simulate ER values for the riffle and pool sequence using distributions from high-zero study
rivers:
# With ability to maipulate either riffle or pool values
RP_ER <- function(River_length = 1000,
            PR_size = 1.2773,   PR_mu = 43.2381,
            RR_size = 1.6393,   RR_mu = 60.1088,
            PR_multiplier = 1, RR_multiplier = 1
){

 n <- River_length/5

 #Prepare output:
 To<- as.data.frame(matrix(0, ncol = 0, nrow = n))
 To$X_coord <-    seq(5, River_length, by = 5)
 To$Pool_ER <-  round(rnbinom(n = n, size = PR_size, mu = PR_mu)*PR_multiplier) #Pools = 0
 To$Riff_ER <-  round(rnbinom(n = n, size = RR_size, mu = RR_mu)*RR_multiplier) #Riffles = 1

 To
}

#Simulate the synthetic stream stretch:
##########################
Temp_RP_sequence <- RP_sequence()
Temp_RP_ER <- RP_ER()

data1D  <- cbind(Temp_RP_sequence, Temp_RP_ER[1], Temp_RP_ER[2], Temp_RP_ER[3])
data1D  <- mutate(data1D, ER = ifelse(Sequence == 0, Pool_ER, Riff_ER), RP = ifelse(Sequence
== 0, "P", "R"))
data1D  <- data1D[, c(4,7,8)] # neat dataset
data1D$River <- "Synthetic_stream_01"

#Plot simulation:
ggplot(data1D, aes(x = X_coord, y = ER, fill = RP))+
 geom_bar(stat="identity", width = 5)
```